NRL/FR/4212—92-9514

A Cloud Chamber Study of the Effect which Nonprecipitating Clouds Have on the Aerosol Size Distribution

G. M. FRICK, W. A. HOPPEL, AND J. W. FITZGERALD

Radio/IR/Optical Sensors Branch
Center for Advanced Space Sensing

AND

B. J. WATTLE

Arvin Calspan Corporation
Buffalo, NY

September 30, 1992

REPORT DOCUMENTATION PAGE

Form Approved
OMB No. 0704-0188

1. AGENCY USE ONLY (*Leave Blank*)	2. REPORT DATE	3. REPORT TYPE AND DATES COVERED
	September 30, 1992	Interim

4. TITLE AND SUBTITLE

A Cloud Chamber Study of the Effect which Nonprecipitating Clouds have on the Aerosol Size Distribution

5. FUNDING NUMBERS

PE - 61153N
PR - RR033-02-42
WU - 1110-0-2

6. AUTHOR(S)

G.M. Frick, W.A. Hoppel, J.W. Fitzgerald, and B.J. Wattle*

7. PERFORMING ORGANIZATION NAME(S) AND ADDRESS(ES)

Naval Research Laboratory
Washington, DC 20375-5320

8. PERFORMING ORGANIZATION REPORT NUMBER

NRL/FR/4212—92-9514

9. SPONSORING/MONITORING AGENCY NAME(S) AND ADDRESS(ES)

Office of Naval Research
Arlington, VA 22217

10. SPONSORING/MONITORING AGENCY REPORT NUMBER

11. SUPPLEMENTARY NOTES

*Arvin Calspan Corporation, Buffalo, NY

12a. DISTRIBUTION/AVAILABILITY STATEMENT

Approved for public release; distribution unlimited.

12b. DISTRIBUTION CODE

13. ABSTRACT (*Maximum 200 words*)

When an air parcel in the atmosphere passes through a nonprecipitating cloud cycle, a subset of the aerosol population called cloud condensation nuclei (CCN) is activated and forms cloud droplets. During the cloud phase, trace gases, such as SO_2, are dissolved into the droplets and undergo aqueous-phase chemical reactions, forming low-volatility products, such as sulfates, which remain as residue when the cloud droplets evaporate. The resulting increase in residual mass can have a dramatic effect on the aerosol size distribution, causing the CCN to grow relative to the smaller particles (interstitial aerosol) which were not activated in the cloud.

This process was graphically demonstrated in a series of experiments carried out in the Calspan 600 m^3 environmental chamber, under conditions where the precloud reactants could be carefully controlled. Size distributions taken before and after a cloud cycle showed significant conversion of SO_2 to H_2SO_4 and a dramatic change in the aerosol size distribution. Subsequent cloud cycles (with the same expansion rate and trace gas concentrations) exhibited very small mass conversion rates. The decreased conversion rate is explained by the increased acidity of the cloud droplet due to the increased mass of the CCN. The terminal size of the resulting CCN was on the order of one-fiftieth the size of the cloud droplets. The pH of a droplet formed on a sulfuric acid aerosol particle one-fiftieth its size is about 5. No such limit to the conversion rate of SO_2 in a droplet was observed when H_2O_2 was used as the oxidant or when gaseous NH_3 was present in sufficient concentration to neutralize the acid.

Growth laws for the increase in the equivalent dry mass of CCN during the time the CCN was within the cloud droplet were derived from the rate of SO_2 conversion in bulk water when the gaseous reactants are in Henry's Law equilibrium with the bulk solution. These growth laws were incorporated into a microphysical cloud model which simulated cloud droplet formation and growth processes in the chamber. The model was initialized using the measured size distribution in the chamber. These modeling results predicted the double peaked character of the size distribution observed in the experiment, but the observed conversion was much greater than that predicted for the case of SO_2 oxidation by O_3.

14. SUBJECT TERMS

Atmospheric aerosols
Atmospheric chemistry

15. NUMBER OF PAGES

51

16. PRICE CODE

17. SECURITY CLASSIFICATION OF REPORT	18. SECURITY CLASSIFICATION OF THIS PAGE	19. SECURITY CLASSIFICATION OF ABSTRACT	20. LIMITATION OF ABSTRACT
UNCLASSIFIED	UNCLASSIFIED	UNCLASSIFIED	UL

NSN 7540-01-280-5500

Standard Form 298 (Rev. 2-89)
Prescribed by ANSI Std 239-18
298-102

CONTENTS

A CLOUD CHAMBER STUDY OF THE EFFECT WHICH NONPRECIPITATING CLOUDS HAVE ON THE AEROSOL SIZE DISTRIBUTION

1. INTRODUCTION

It is well known that background aerosol affects cloud microstructure, and hence influences cloud optical properties and radiative transfer, a subject of great interest in climate research. Cloud droplets form on preexisting aerosol particles called cloud condensation nuclei (CCN). Whether or not an aerosol particle will act as a CCN in a given cloud depends in a complicated way on the cooling rate, and the number, size distribution, and composition of the particles. For the composition of particles typically found in the atmosphere, particles larger than about 0.03 to 0.08 μm radius (depending on the maximum cloud supersaturation) will be activated in typical clouds.

Less understood and less recognized is the fact that nonprecipitating cloud cycles are a significant factor in shaping the background aerosol size distribution. More than 90% of the clouds in the atmosphere (Pruppacher 1986) reevaporate without the formation of precipitation. This means that a parcel of air will be processed through many nonprecipitating clouds (on average) before it is incorporated into a precipitating cloud where the aerosol can be removed by precipitation scavenging. The cloud droplet radius (mass) is approximately 100 (10^6) times larger than that of the "dry" CCN. During the cloud phase, the droplet can absorb soluble trace gases (e.g., sulfur dioxide and oxides of nitrogen) and oxidants (e.g., ozone and hydrogen peroxide) which react in the liquid phase to form less volatile products that remain as residue after the cloud evaporates, thus causing an increase in aerosol mass. In an early paper, Hobbs (1971) suggested that the production of sulfates in cloud droplets, followed by the release of these particles when the droplet evaporates, could be an important mechanism for increasing the efficiency of CCN. In a subsequent paper, Hegg et al. (1980) found an increase in the concentrations of CCN downwind of a wave cloud and an increase in the sulfate load of about 0.5 μg m^{-3} from filter samples. Measurements of the particle size distribution at radii greater than about 0.25 μm with an optical particle counter suggested that particles of about 0.5 μm were responsible for the increase. However, the size distribution data was much less convincing than the CCN and filter loading data and probably did not go to sufficiently small sizes to see the region where most conversion occurs. In addition to conversion within the cloud droplets, smaller unactivated particles (interstitial aerosol) will diffuse to the large surface area provided by the cloud droplets. The mass of the smaller particle is incorporated into the CCN after evaporation. The former process (i.e., a liquid phase reaction) has a much larger effect on the mass of CCN than does the latter.

The growth of CCN mass during nonprecipitating cloud cycles has a tendency to produce a separation in the size distribution at the critical particle radius which corresponds to the supersaturation in the cloud. Hoppel et al. (1983, 1986, 1990) hypothesized that this mechanism caused the double-peaked size distribution which they observed in the 0.01 to 0.2 μm size range in the marine boundary layer. The minimum between the two peaks is between 0.06 to 0.1 μm radius. This persistent double-peaked feature is observed both over the Atlantic (Hoppel et al. 1990) and Pacific Oceans (Hoppel and Frick 1990). While the double-peaked feature is not as conspicuous over land, we believe

Manuscript approved July 13, 1992.

nonprecipitating clouds play an equal, if not more important, role in supplying aerosol mass over continental regions. The minimum between the two peaks is obscured by locally distributed sources over continental regions and the fact that the relationship between size and critical supersaturation is less well defined for continental aerosol whose composition is less well defined. However, there is often a large amount of mass created in the 0.1 to 0.5 μm radius range over continents which, under some circumstances, is best explained in terms of the nonprecipitating cloud process.

This report describes experiments carried out in Calspan's 590 m^3 chamber to study the effect of nonprecipitating clouds on the aerosol size distribution under well-controlled conditions. The use of a very large chamber is required because cloud droplets which are of the order of 10 μm will fall about 3 m in 5 minutes. The change in the aerosol size distribution during a cloud cycle which resulted from the liquid phase oxidation of SO_2 by ozone in cloud droplets was measured and the results compared to those obtained by modeling. Oxidation of SO_2 by hydrogen peroxide during a cloud cycle was also observed but a detailed quantitative comparison with theory is not possible because no capability was available to measure hydrogen peroxide concentrations.

2. AEROSOL GROWTH LAWS FOR LIQUID PHASE CONVERSION OF SULFUR DIOXIDE TO SULFATE IN CLOUD DROPLETS

From the rate at which trace gases and oxidants react in the cloud droplet to form involatile products, growth laws for the equivalent "dry" size can be derived. This can be done provided the following are known:

- the liquid phase reaction rates,
- the gas phase concentrations of the reactants,
- the Henry's law constants,
- the cloud droplet size, and
- the composition of the CCN.

2.1 Growth Law for the Oxidation of Sulfur Dioxide by Ozone in a Cloud Droplets

The rate of oxidation of SO_2 by O_3 in bulk water which is in Henry's law equilibrium with SO_2 and O_3 in the surrounding air is given by Hoffmann (1986) as

$$\frac{d[SO_4]}{dt} = \left\{ k_o + k_1 \frac{K_1}{[H^+]} + k_2 \frac{K_1 K_2}{[H^+]^2} \right\} H_O H_S P_O P_S \tag{1}$$

where $[SO_4]$ is the concentration of sulfate in moles l^{-1}, $[H^+]$ is the hydrogen ion concentration in moles l^{-1}, H_O and H_S are the Henry's law constants (moles l^{-1} atm^{-1}); P_O and P_S are the ambient vapor pressures for ozone and sulfur dioxide in atmospheres; k_0, k_1, and k_2 are the rate constants for reaction of O_3 with $SO_2 \cdot H_2O$, HSO_3^-, and SO_3^{2-}, respectively; and K_1 and K_2 are the first and second dissociation constants for dissolved SO_2 in moles l^{-1}.

In terms of the total conversion rate in a droplet of radius R (in cm), Eq. (1) becomes

$$\frac{d[SO_4]}{dt} = 6.75 \times 10^{-5} \left\{ \frac{4.81 \times 10^3}{[H^+]} + \frac{1.174}{[H^+]^2} \right\} R^3 P_O P_S \tag{2}$$

where $[SO_4]$ is the moles of sulfate in the droplet. In Eq. (2), values of the constants for T = 25° C given by Hoffmann (1986) and Jacob and Hoffmann (1983) have been adopted and the first term on the right of Eq. (1) has been dropped because it has a negligible effect on the growth rates. Assuming complete ionization of sulfuric acid ($H_2SO_4 \rightarrow H^+ + HSO_4^-$), the hydrogen ion concentration and the moles of sulfate in the droplet can be expressed in terms of the mass of sulfuric acid M_a as

$$[H^+] \approx 2.436 \frac{M_a}{R^3} \tag{3}$$

and

$$[SO_4] = \frac{M_a}{M_w} \tag{4}$$

where M_w is the molecular weight of sulfuric acid. Equation (3) is valid only when the pH is less than about 6.5. The mass growth rate of sulfuric acid in a cloud droplet can then be expressed as

$$\frac{dM_a}{dt} = \left[\frac{13.06}{M_a} + \frac{1.31 \times 10^{-3} R^3}{M_a^2}\right] R^6 P_O P_S. \tag{5}$$

Equation (5) can be integrated so that the acidic mass at a later time can be found for a droplet of fixed radius in an atmosphere of known SO_2 and O_3 concentrations.

The two terms on the right of Eqs. (2) and (5) are equal when the pH of the droplet is about 3.6. For most calculations, only the $[H^+]^{-2}$ term is important. This is because at low pH (high $[H^+]$ concentrations), the growth is negligible on the time scale of interest in this study. For higher pH where growth rates are significant, the second term makes the dominant contribution. If only the second term is retained, integration yields

$$M_a^3(t) = M_a^3(0) + 3.92 \times 10^{-3} R^9 P_O P_S t \tag{6}$$

where $M_a(0)$ is the initial mass of the sulfuric acid in the droplet.

Since sulfuric acid is hygroscopic, even at low relative humidities (RH), it is convenient to write the initial mass of sulfuric acid in terms of the total initial mass $M_T(0)$ (at some reference relative humidity) as

$$M_a(0) = c\epsilon M_T(0) \tag{7}$$

where c is the weight fraction of the sulfuric acid in solution at the reference RH, and ϵ the fraction of acidic solution in the particle. Thus, $(1-\epsilon)M_T(0)$ represents the fraction of nonacidic material in the original CCN.

Likewise, if $M_T(t)$ is the total "dry" mass of the particle at time t (i.e., the mass remaining in the droplet after evaporating to its equilibrium size at the reference humidity), then

$$M_a(t) = c[M_T(t) - (1-\epsilon)M_T(0)] \tag{8}$$

where, for lack of a better assumption, we have assumed that the nonacidic fraction has the same hygroscopicity as does the sulfuric acid.

The reference relative humidity is taken to be the relative humidity in the differential mobility size spectrometer. Equation (6) can then be written as

$$\left[cM_T(T) - c(1-\epsilon)M_T(0)\right]^3 = \left[c\epsilon M_T(0)\right]^3 + 3.92 \times 10^{-3} R^9 P_O P_S t. \tag{9}$$

If the original CCN were totally acidic ($\epsilon = 1$), Eq. (9) could be written in terms of the radius as

$$\left[\frac{r(t)}{R}\right]^9 = \left[\frac{r(o)}{R}\right]^9 + \frac{3.92 \times 10^{-3}}{(4/3\ \pi \rho_a c)^3} P_O P_S\ t \tag{10}$$

where r is the "dry" radius and ρ_a is the density of the acid at the reference RH. The radial growth law can then be written as

$$\frac{dr}{dt} = \frac{1.31 \times 10^{-3}}{3\ (4/3\ \pi\ \rho_a\ c)^3} \frac{R^9}{r^8} P_O P_S. \tag{11}$$

It is evident that the growth rate increases very rapidly with increasing cloud droplet radius (R^9) and decreases rapidly with increasing particle radius (r^{-8}). This decrease with increasing particle radius is much more rapid than any of the proposed gas-phase growth laws (McMurry and Wilson 1982). (The most rapidly decreasing gas-phase growth law is for diffusional growth and is proportional to r^{-1}.) Once the growth rate reaches a threshold where the rate is observable on the time scale of the experiment, further increase of R dramatically increases the growth rate of r, so that r then tracks the increase in the cloud droplet radius R. Physically, this tracking is largely caused by the pH effect of the reaction. As the cloud droplet radius increases, dilution occurs, increasing the pH; the reaction rate increases again, lowering the pH and slowing the conversion rate.

This tracking is better illustrated by Eq.(10). If there is any significant growth, then $r^9(t) >> r(0)^9$ and Eq. (10) becomes

$$\frac{r(t)}{R} = \left[\frac{5.34 \times 10^{-5}}{(\rho_a c)^3} P_O P_S\ t\right]^{1/9} = 0.38(P_O P_S\ t)^{1/9}. \tag{12}$$

Values of $c = 0.5$ and $\rho_a = 1.4$, corresponding to our reference humidity of 34% (humidity in the DMA size spectrometer), have been used in Eq. (12).

The dependence of the ratio $r(t)/R$ on P_O, P_S, and time in the cloud is very weak. For conditions typical of those in our experiments ($P_O = 90$ ppb, $P_S = 6$ ppb, and $t = 240$ s), this ratio becomes

$$\frac{r}{R} = 0.137. \tag{13}$$

Changing P_S, P_O, t or their product by an order of magnitude changes this ratio by less than 30%. This ratio corresponds to a pH in the droplet of about 4.5. For 5 to 10 μm cloud droplets, this corresponds to dry radii of 0.07 to 0.14 μm.

Figure 1 shows solutions to Eq. (10) for three cloud droplet radii (R = 4, 6, and 8 μm). The time in cloud is 4 min. Nuclei larger than about 0.15 μm do not grow even in the 8 μm radius cloud droplet because the low pH caused by the original nucleus is sufficient to turn off the conversion of SO_2. Drops which form on small nuclei are sufficiently dilute (high pH) that conversion of SO_2 can occur. Figure 2 shows the growth of the "dry" size as a function of time as calculated from Eq. (10), starting with a nucleus whose radius is 0.04 μm. The growth is initially very rapid in the larger droplet but is quickly diminished as the pH of the droplet is decreased by conversion of SO_2 to sulfuric acid.

The above arguments are for acidic nuclei. For nonacidic nuclei, acidic mass can be formed before the pH is sufficiently low to quench the conversion. For the case of a nonacidic nucleus (ϵ = 0), Eq. (9) becomes

$$\left[\frac{r(t)}{R}\right]^3 = \left[\frac{r(o)}{R}\right]^3 + \left\{\frac{3.92 \times 10^{-3}}{(4/3\ \pi\ \rho_a c)^3}\ P_O P_S\ t\right\}^{1/3} \tag{14}$$

where the density ρ_o of the nonacidic material is assumed to be the same as that of the sulfuric acid at the reference relative humidity and to have the same concentration of associated water. Figure 3 shows the change in the "dry" radius before and after a cloud for the same conditions as in Fig. 1 except that here the starting nuclei are not acidic.

2.2 Growth Law for Oxidation of Sulfur Dioxide by Hydrogen Peroxide in a Cloud Droplet

The rate of sulfate formation due to aqueous-phase oxidation of SO_2 by H_2O_2 can be written (Overton 1985) as

$$\frac{d[SO_4]}{dt} = k\,[H_2O_2]\,[S(IV)] \tag{15}$$

where $S(IV)$ is the sulfur dioxide in the water as hydrated sulfur dioxide, bisulfite ion, and sulfite ion; and k is the effective second-order rate constant for the H_2O_2 - $S(IV)$ reaction. Since

$$[S(IV)] = [SO_2(aq)]\left\{1 + \frac{K_1}{[H^+]} + \frac{K_1K_2}{[H^+]^2}\right\}, \tag{16}$$

we have

$$\frac{d[SO_4]}{dt} = k\left\{1 + \frac{K_1}{[H^+]} + \frac{K_1K_2}{[H^+]^2}\right\} H_S H_H P_S P_H \tag{17}$$

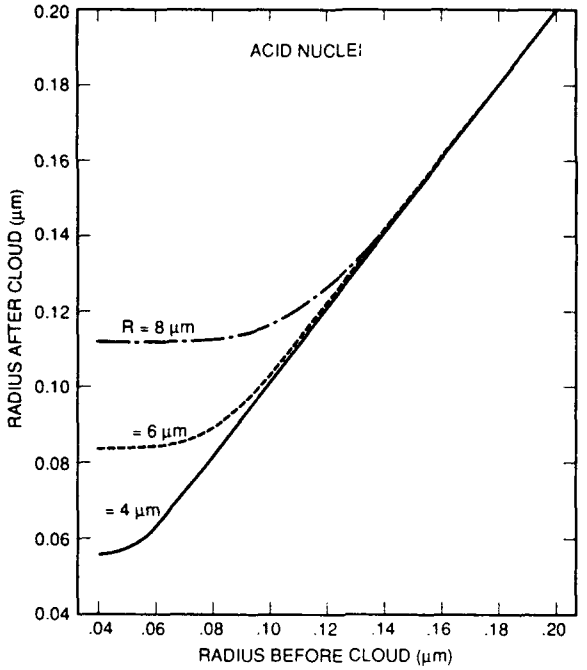

Fig. 1 — Growth of "equivalent dry radius" of nucleus during a 4 min cloud cycle for cloud droplets of 4, 6, and 8 μm radius. SO_2 and O_3 concentrations are 6 ppb and 90 ppb, respectively. The equivalent dry radius is taken to be the radius of a sulfuric acid nucleus at 34% RH.

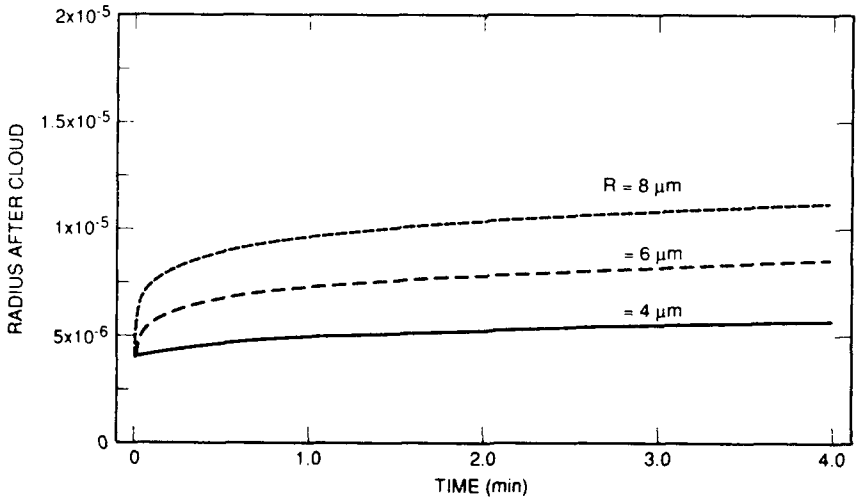

Fig. 2 — Growth of equivalent dry radius as a function of time in cloud droplets of 4, 6, and 8 μm radius. Conditions are the same as in Fig. 1.

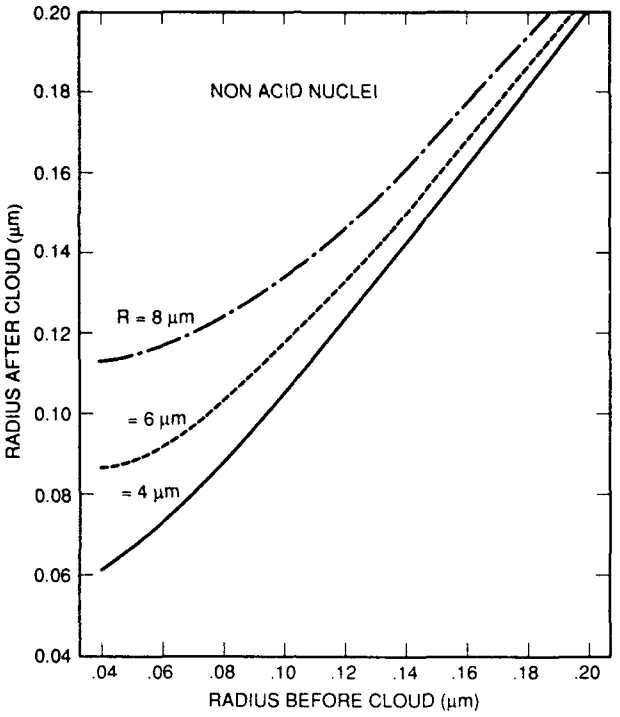

Fig. 3 — Same as Fig. 1 except here the starting nucleus is assumed to be nonacidic

where H_H and H_S are Henry's Law constants for H_2O_2 and SO_2, respectively, and P_H and P_S are the environmental pressures of H_2O_2 and SO_2 in atmospheres. If we adapt Overton's (1985) expression for k, the product of k and $(1+K_1/[H^+]+K_1K_2/[H^+]^2)$ has a nearly constant value of 7.7×10^5 s^{-1} atm^{-1} for pH values greater than about 2.0. Evaluating Eq. (17) and using $H_H = 9.7 \times 10^4$ moles l^{-1} atm^{-1} (Chameides 1984) and $H_S = 1.24$ moles l^{-1} atm^{-1} gives

$$\frac{d[SO_4]}{dt} = 9.3 \times 10^{10} P_H P_S. \tag{18}$$

Converting Eq. (18) from moles per liter to moles per droplet where the droplet has a radius of R gives

$$\frac{d[SO_4]}{dt} = \frac{4/3\pi}{1000} (9.3 \times 10^{10}) R^3 P_H P_S. \tag{19}$$

Using Eq. (4) to convert moles of sulfate to total mass of sulfuric acid M_a in the droplet, Eq. (19) becomes

$$\frac{dM_a}{dt} = 3.9 \times 10^{10} R^3 P_H P_S. \tag{20}$$

Since the conversion rate is proportional to R^3, the conversion of SO_2 by H_2O_2 is expected to be proportional to the liquid water content of the cloud provided the reactants are not depleted; this was not the case for liquid-phase conversion of SO_2 by ozone. Integration of Eq. (20) yields

$$M_a(t) = M_a(o) + 3.9 \times 10^{10} R^3 P_H P_S t. \tag{21}$$

Converting acidic mass in Eq. (21) to total "dry" mass by using Eq.(8), we obtain

$$M_T(t) = M_T(o) + \frac{3.9 \times 10^{10}}{c} R^3 P_H P_S t. \tag{22}$$

In terms of radius

$$\frac{r(t)}{R} = \left[\left[\frac{r(o)}{R} \right]^3 + \frac{3.9 \times 10^{10}}{4/3 \pi \rho_a c} P_H P_S t \right]^{1/3} \tag{23}$$

where, for simplicity, we have assumed that the nonacidic component in the original nuclei has approximately the same density as the acid at the reference humidity. In this case, the radial growth law is given by

$$\frac{dr}{dt} = \frac{3.9 \times 10^{10}}{4 \pi \rho_a c} \frac{R^3}{r^2} P_H P_S. \tag{24}$$

The growth rate is proportional to the volume of the cloud droplet and inversely proportional to r^2.

Figure 4 shows the growth of the equivalent dry radius at the reference RH over a period of 4 min in cloud droplets of 4, 6, and 8 μm radius, similar to that shown in Fig. 2 for O_3 oxidation. For the H_2O_2 oxidation, the same SO_2 concentration of 6 ppb was used but the H_2O_2 concentration was assumed to be only 1 ppb. Still, the growth for the H_2O_2 oxidation of SO_2 is much faster than with 90 ppb of ozone.

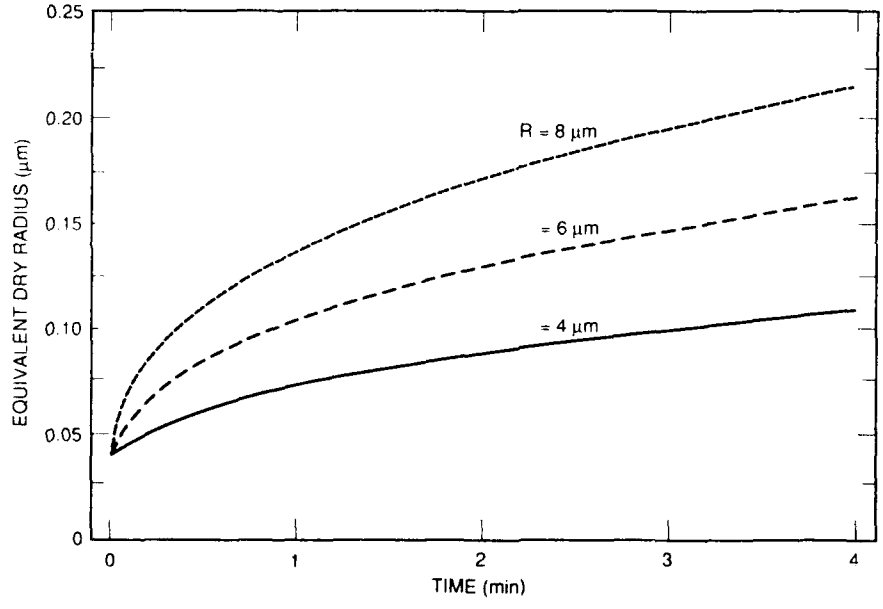

Fig. 4 — Growth of equivalent dry radius in cloud droplets of 4, 6, and 8 μm radius for the case of 6 ppb SO_2 and 1 ppb H_2O_2

Figure 5 compares the radius of the CCN before and after a 4 min cloud cycle for the conditions stated above (P_H = 1 ppb). Here the growth is not limited by the pH.

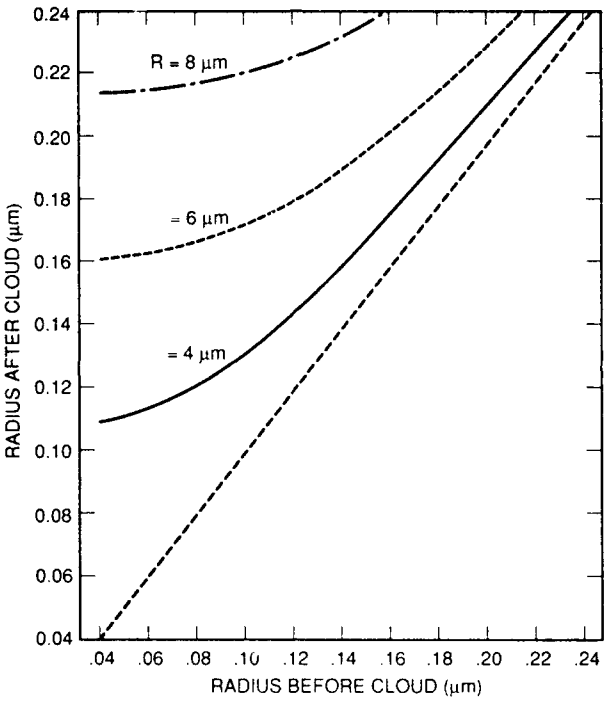

Fig. 5 — Growth of equivalent dry radius of nucleus during a 4 min cloud cycle for oxidation by H_2O_2. SO_2 and H_2O_2 concentrations were taken to be 6 ppb and 1 ppb, respectively.

If $r^3 >> r_o^3$, then the equivalent dry radius is proportional to the cloud drop radius and to the cube root of the time (Eq. (23)). From Eqs. (3) and (21) it is obvious that the pH in the droplet is inversely proportional to the time and independent of the radius of the cloud droplet; hence, $[H^+] = 9.5 \times 10^{10} P_H P_S t$.

For the conditions cited and 4 min in a cloud the pH is about 3.9. (When pH drops below about 3.0, our original assumption that the product $k(1+K_1/[H^+]+K_1K_2/[H^+]^2)$ is constant would not be valid.)

It must be remembered that the assumed conditions of a cloud droplet growing in an environment of constant reactant gases is unrealistic because the 1 ppb of H_2O_2 would rapidly be used up and the conversion would cease (by the time about 4 μg m^{-3} of sulfate aerosol were formed)

2.3 Depletion of Reactants

The above analysis assumes constant concentrations of reactants. During the conversion process, the reactants are depleted; for example, the conversion of 1 ppb of SO_2 will produce about 4.4 μg m^{-3} of sulfuric acid. For the case of SO_2 - O_3, the rate of growth depends only weakly on the concentrations of the reactants (see Eq. (11)) until one of the reactants is nearly depleted. If one mole of gaseous reactant j produces one mole of sulfate of molecular weight M_w, then the decrease in vapor pressure P_j (in atmospheres) will produce an increase in sulfate mass density ρ_s (in g cm^{-3}) given by

$$dP_j = \frac{2.24 \times 10^4}{M_w} d\rho_s. \tag{25}$$

For example, 1 ppb change in SO_2 would produce approximately 4.4 $\mu g\ m^{-3}$ of sulfuric acid. In terms of the mass of a single particle M_a

$$\frac{dP_j}{dt} = - \frac{2.24 \times 10^4}{M_w} Z \frac{dM_a}{dt} \tag{26}$$

where Z is the number density of cloud droplets. If depletion is significant, then Eq. (26) must be coupled with Eq. (5) for SO_2-O_3 conversion or with Eq. (17) for SO_2-H_2O_2 conversion. Depletion of reactants due to in-cloud conversion in our chamber experiments were not important for the cases of SO_2 oxidation of ozone. However, in the real atmosphere where reactant concentrations can be extremely low, depletion may be the limiting factor as discussed in the conclusions of this report.

3. DESCRIPTION OF INSTRUMENTS AND PROCEDURES

In October and November of 1990, a series of experiments were carried out in Calspan's 590 m^3 environmental chamber where the reactants could be carefully controlled. The purpose of the experiments was twofold:

- to measure the change in the aerosol size distribution caused by the liquid-phase conversion of SO_2 to sulfate in cloud droplets during a cloud cycle, and
- to measure gas-phase photolysis rate of DMS and SO_2 under controlled conditions.

This report describes only the cloud cycling experiments, together with a comparison of measured and modeled results.

3.1 Calspan Environmental Chamber

The Calspan chamber is a cylinder 9.14 m high enclosing a volume of 590 m^3 (20,800 ft^3). The 1.25-cm-thick steel walls of the chamber are designed to withstand pressure differentials of 60 kPa (kilopascals) (600 mb); however, the Pyrex cover plates of the irradiation system currently limit pressure differentials to about 40 cm of water (39 mb). The maximum pressure differential was only about 20 mb in the set of experiments discussed here. The inner chamber surface is coated with a fluoroepoxy type urethane developed at NRL, which has surface energy and reactivity properties comparable to those of FEP Teflon. Illumination for photochemical experiments within the chamber is provided by 28.6 kW of fluorescent blacklight and sunlamps installed inside 24 lighting modules and arranged in eight vertical channels attached to the wall of the chamber.

In 1990, prior to this set of experiments, the ultraviolet irradiation system was refurbished by replacing both the fluorescent lights and black lamps. Subsequent to the experiments, measurements were made of the relative spectral irradiance in the chamber. The spectrum showed a peak irradiance at 350 nm and half-power points at ± 20 nm.

The chamber light intensity as monitored by photodissociation of NO_2 in air gave a $k_1 = (NO_2)_o^{-1} (d0_3/dt)_{t=0}$ (Wu and Niki 1975) of 0.39 min^{-1}. This value compares to $k_1 = 0.325\ min^{-1}$, with probable error of $\pm 15\%$, computed from the photostationary state of [NO], [O_3], and [NO_2].

Absolute aerosol filters are used for removal of aerosol particles before and after the activated charcoal filters (300 lbs of charcoal). The air handling capability made it possible to reduce the Aitken nucleus count to less than 10 cm^{-3} and to remove those gaseous contaminants which can be removed by charcoal filtering. A tube with many small holes around the top of the chamber was used to direct small

streams of distilled water down the sides of the Teflon-coated walls to humidify the chamber. A large (low RPM) fan in the chamber provides circulation (when desired) to maintain uniform conditions within the chamber. Figure 6 shows the interior of the chamber. The chamber has an airlock for personnel and large instrumentation as well as several observation and sampling ports. The temperature of the chamber is largely determined by the temperature within the building. The air-handling system is such that the half-time for reducing aerosol concentrations and trace gas concentrations is about 20 min.

Fig. 6 — Interior of Calspan's 590 m³ environmental chamber

3.2 Aerosol Instrumentation

The NRL Differential Mobility Analyzer (DMA) was built at NRL and is described in detail in Hoppel (1978) and Hoppel et al. (1983). The DMA system has since been modified to operate in a scanning mode (Wang and Flagan 1990) with an inversion scheme that provides 44 fixed channels between 0.005 and 0.531 microns radius. A TSI model 3022 Condensation Particle Counter (CPC) with butanol working fluid is used to count the transmitted particles. A HP 9845C computer is used for control, data acquisition, and inversion tasks.

The DMA aerosol sample intake was approximately one meter from the chamber wall, and the sample immediately passed through a diffusion dryer to shrink the particles to their size at about 80% relative humidity. The reduction in the size of a sulfuric acid particle when the relative humidity is lowered from 100% to 80% is more than a factor of two in radius and a factor of eight in mass. The DMA sheath air was also dried as it was recycled, maintaining a dew point of approximately 4° C. Sampling from the chamber at over-pressure with the DMA required the CPC makeup air port and butanol supply bottle vent to be plugged to maintain proper flow (5 cm^3 s^{-1}) through the CPC and stop air from escaping by bubbling through the butanol supply line.

Cloud droplet size spectra were measured with a Particle Measuring Systems Inc., Classical Scattering Aerosol Spectrometer Probe, Model 100 (PMS CSASP-100) located within the chamber approximately two meters from the wall. Droplet spectra were obtained every 20 s using only the largest CSASP range which consisted of 15 channels, specified to be 0.6 μm in width and to span the range from 1.0 to 10.0 μm in radius. The factory calibration used two sizes of glass spheres (3 to 5 and 10 to 15 μm dia.) with complex index of refraction m = 1.51-0i (at λ = 0.5893 μm) to calibrate this range of the instrument, which uses a He-Ne laser operating at a wavelength of 0.6328 μm. Glass beads and water have different refractive indices. Based on the work of Pinnick and Auvermann (1979), errors of 20% and larger are anticipated for certain radii in the size range of interest due to the differences in the index of refraction.

A second TSI model 3022 CPC monitored the condensation nuclei concentration in the chamber, which was recorded every 10 s together with temperature, pressure, and dew point.

3.3 Chamber Equipment and Instrumentation

3.3.1 Ozone Generator

The ozone generator is a Model T-408 ozonator built by Wesbach Ozone System Corp. and now handled by Polymetrics of Pleasanton, CA. Ozone was generated in these experiments by feeding oxygen rather than air into the ozonator. The amount of ozone generated from O_2 is between 1.7 and 8% by weight depending on the O_2 flow rate, primary voltage, and temperature of the cooling medium. Thus the ozone generator supplies only O_3 and residual O_2 to the chamber.

3.3.2 Sulfur Dioxide Monitor

Sulfur dioxide was monitored with a Thermo Environmental Instruments Inc. Model 43S High Sensitivity Pulsed Fluorescence SO_2 Analyzer. This instrument has a lower detectable limit of 0.1 ppb SO_2 and a rejection ratio for NO of approximately 50:1.

3.3.3 Liquid Water Content Measurement

The liquid water content of the fogs generated in the chamber was measured via extinction at an infrared wavelength of 11 μm (Chylek 1978). The IR beam enters the chamber with intensity I_o, traverses the chamber diameter, is reflected at the far wall, and returns to the detector (a total distance of approximately 19 m) where the intensity I is measured. The liquid water content is then computed from the extinction as determined by I/I_o.

3.3.4 Ion Chromatography

Ion chromatography was performed on filter samples to detect sulfate, nitrate, ammonium ions, and methane sulfonic acid. The filters are 90 mm in diameter and were exposed at a nominal flow rate of 1 m^{-3} min^{-1} for 10 min, thus giving a total volume of approximately 10 m^{-3}. The collected aerosol was then dissolved from the filter with deionized water and the resulting solution was injected into an ion chromatograph.

Calspan chamber instrumentation also included the following where the minimum detectable limit is included in parentheses:

- Bendix Model 8002 Ozone Analyzer (1 ppb)
- Bendix Model 9101-B Nitrogen Oxide Analyzer for NO and NO_2 (5 ppb)

- Meloy Model 5A260 Flame Photometric Total Sulfur Gas Analyzer (0.5 ppb)
- Bendix Model 8201 Reactive Hydrocarbon Analyzer for methane, total hydrocarbon and reactive (non-methane) hydrocarbons (5 ppb)

3.4 Typical Cloud-Cycle Procedure

The generation of the background aerosol, humidification of the chamber, and subsequent cloud formation for each of the cloud experiments followed a similar pattern. Overnight the air in the chamber was continuously filtered to remove aerosol and trace gases. When the experiment began in the morning, the SO_2, O_3 and NO_x concentrations were below the limits of detection (0.2 ppb, 2 ppb, and 1 ppb, respectively). The charcoal filters did not remove methane and were not very effective in removing non-methane hydrocarbons (NMHC). NMHC concentration was usually, but not always, below the ambient levels. Known concentrations of O_3 and SO_2 were then introduced into the chamber. Typical values were $[SO_2]$ = 15 ppb and $[O_3]$ = 100 ppb. This produced a copious supply of small particles which grew into the size range which could be detected with the DMA in about 20 min. The particles were then allowed to grow until the desired size distribution was obtained. This usually took about 1 to 2 hours. Over this growth period, there was always significant loss of ozone, presumably as a result of wall losses. To sustain the aerosol growth rate, additional O_3 was on most occasions added to the chamber; on a few occasions, additional SO_2 was also added. The growth rate could be increased substantially by adding NMHC in the form of propene. The growth occurred at about the same rate whether or not the lamps (which simulated the solar spectrum) were on. Therefore the lamps were left off to prevent heat accumulation in the chamber. Since the reaction occurred in the dark and NMHC were always present at concentrations greater than several hundred ppb, it was assumed that the SO_2 was converted to sulfuric acid aerosol by the Criegee intermediate process (see, for example, Finlayson-Pitts and Pitts 1986). The ozone reacts with the NMHC forming Criegee intermediates which oxidize the SO_2. Figure 7 shows the process of forming the initial aerosol size distribution. In this case, the beginning concentrations of O_3 and SO_2 were 120 ppb and 15 ppb, respectively. The first size distribution was taken 20 min after adding reactants to the chamber, and the subsequent size distributions were taken 10, 20, 30, 50, and 70 min after the first size distribution.

As will be evident later, the effect of in-cloud conversion is most readily observed when the initial size distribution is very steep in the size range containing the smallest particle to be activated in the cloud.

After the desired size distribution was obtained, the chamber was filtered to decrease the concentrations of the reactants and aerosols. The chamber air was typically filtered for about 40 min to an hour and the concentrations were reduced by about a factor of 5. This reduction in the reactant concentration slowed further growth of the particles. The chamber was then humidified by passing distilled, deionized water down the wall, forming puddles on the floor. After about half an hour, when the dewpoint depression was less than 1° C, the levels of SO_2 and O_3 desired for the cloud cycling experiment were added to the chamber. The amount of additional SO_2 needed to obtain the targeted concentration was always considerably greater than that calculated. This was attributed to loss of SO_2 to the walls and to the water on the floor and walls of the chamber. (Typically, the amount of SO_2 required to produce 5 ppb would have produced 30 ppb in the chamber if there were no surface losses.) The mixing fan ran continuously in the chamber except during the cloud phase. The fan was turned off just prior to expansion (cloud formation). When the desired concentrations of gas-phase reactants were achieved the chamber was overpressured to approximately 15 mb and held there for about 5 min; at the end of 5 min, the measured dew point depression was typically 0.6° C.

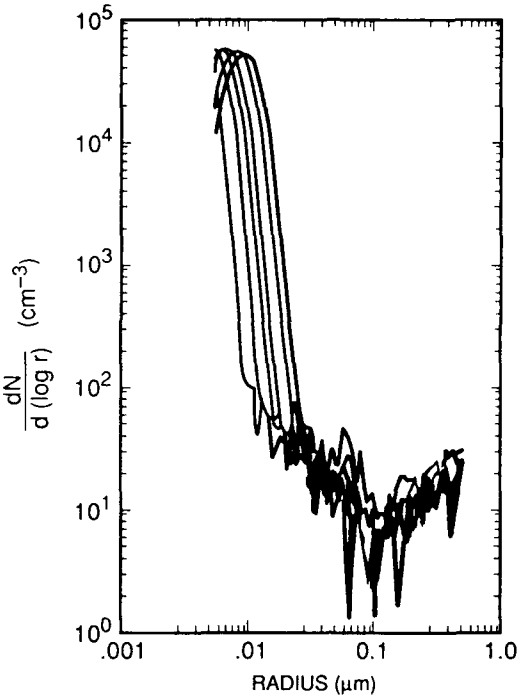

Fig. 7 — Formation of initial aerosol size distribution prior to cloud formation. Beginning SO_2 and O_3 concentrations were 15 ppb and 120 ppb, respectively. First size distribution was taken 20 min after adding reactants; subsequent size distributions were taken at 10, 20, 30, 50, and 70 min after the first distribution.

Since the dew point measurement at these high humidities has an accuracy of about 0.3° C, the dew point depression was in the range 0.6° ± 0.3° C. The chamber was then expanded by exhausting air, and a cloud formed. The expansion was continued until the pressure was about 5 mb below atmospheric pressure by using the chamber exhaust fan. The expansion rate was varied between experiments and was not constant with time. Typically, a 15 mb expansion was completed in about 50 s. The pressure was recorded digitally every 10 s, and was also recorded on a strip chart recorder.

After expansion the cloud was held for about 4 min to allow for liquid-phase conversion of SO_2. During this time, the cloud droplet size spectrum was measured with an optical particle spectrometer every 30 s. After about 3 min, the cloud would start to thin at the top of the chamber and near the walls. After holding the cloud for about 4 min, the chamber would be recompressed with filtered air and the size distribution would be measured and compared to the size distribution prior to the cloud.

This cloud cycling process would then be repeated on the same air using different values of the reactant concentrations and expansion rates.

4. RESULTS OF CLOUD-CYCLING EXPERIMENTS

Table 1 lists 12 cloud cycling experiments in chronological order and are designated as data sets B through N. On November 1, 2, and 9 (ten data sets), the in-cloud oxidation of SO_2 by O_3 was studied. In-cloud oxidation of SO_2 by H_2O_2 was studied on November 10. On each of these days, multiple cloud cycles were performed on the same air. The cycle number is listed in the CCY column. The table gives the measured SO_2 and O_3 concentrations and indicates when NH_3 and H_2O_2 were added to the chamber.

Table 1 — Experimental and Modeled Data

1a. EXPERIMENT RESULTS

SET	DATE	TIME	CCY	REACTANTS (ppb) SO2	O3	OTHER	AEROSOL MASS (ug/m3) BEFORE	AFTER	CHG	CRIT. RAD. (um)	CRIT. SS (%)	CONVERSION PER DROP (femtograms)	LWC (g/m3) IR	LWC (g/m3) PMS/DMA	DROPLET CONC. (cm-3) DMA	CSASP DROPLET RADIUS (um) FACTORY	PINNICK
B	11/01	1550	1	6.5	107		0.95	7.35	6.40	0.040	0.315	4.57	0.220	0.690	1400	4.6 - 5.2	4.6 - 4.9
C	11/01	1656	2	5.5	68		7.69	8.09	0.40	0.070	0.136	0.40	0.144	0.493	1000	4.6 - 5.2	4.6 - 4.9
E	11/02	1327	1	4.0	78		1.89	5.52	3.63	0.050	0.226	27.92	0.125	0.334	130	8.2 - 8.8	7.0 - 7.5
F	11/02	1507	2	7.5	74		4.28	5.99	1.71	0.045	0.264	2.85	0.111	0.296	600	4.6 - 5.2	4.6 - 4.9
G	11/02	1606	3	8.0	83		7.28	8.45	1.17	0.085	0.102	3.34	0.093	0.172	350	4.6 - 5.2	4.6 - 4.9
H	11/09	1320	1	5.5	82		1.08	11.40	10.32	0.040	0.315	6.88	0.180	0.318	1500	3.4 - 4.0	3.2 - 4.0
I	11/09	1450	2	4.5	88		14.10	18.70	4.60	0.090	0.093	6.57	0.150	0.345	700	4.6 - 5.2	4.6 - 4.9
J	11/09	1610	3	?	76	NH3	24.30	97.50	73.20			56.31	0.220	0.641	1300	4.6 - 5.2	4.6 - 4.9
K	11/09	1927	1	0.3	2	RURAL	5.43	4.81	-0.62			0.00	0.151			4.6 - 5.2	4.6 - 4.9
L	11/09	2023	2	6.1	75	RURAL	4.96	12.10	7.14	0.055	0.196	8.93	0.195	0.445	800	4.9 - 5.3	5.2 - 5.8
M	11/10	1232	1	3.5	15	H2O2	1.18	24.30	23.12	0.045		243.37		0.244	95	8.2 - 8.8	7.0 - 7.5
N	11/10	1441	2	4.8	5	H202	12.70	26.90	14.20	0.040		71.00		0.514	200	8.2 - 8.8	7.0 - 7.5

1b. MODELED RESULTS

SET	DATE	TIME	CCY	REACTANTS (ppb) SO2	O3	OTHER	AEROSOL MASS (ug/m3) BEFORE	AFTER	CHG	ACTIVE RADIUS (um)	MAX SS (%)	CONVERSION PER DROP (femtograms)	CHG (new K)	LWC (g/m3)	DROPLET CONC. (cm-3)	DROPLET RADIUS (um)
B	11/01	1550	1	6.0	90.0		0.95	1.57	0.63	0.033	0.350	0.48	2.012	0.265	1297	4.4 - 4.7
C	11/01	1656	2	6.0	90.0		7.69	7.70	0.01	0.060	0.187	0.00		0.161	1345	3.2 - 3.7
E	11/02	1327	1	6.0	90.0		1.89	2.93	1.04	0.041	0.323	9.90	2.880	0.318	105	8.8 - 8.9
F	11/02	1507	2	6.0	90.0		4.28	4.46	0.18	0.041	0.324	0.40		0.179	460	5.7 - 5.8
G	11/02	1606	3	6.0	90.0		7.28	7.30	0.02	0.049	0.232	0.03		0.187	655	4.1 - 4.3
H	11/09	1320	1	6.0	90.0		1.08	2.06	0.98	0.030	0.400	0.62	11.11	0.350	1580	4.6 - 4.9
I	11/09	1450	2	6.0	90.0		14.10	14.10	0.00	0.067	0.161	0.00		0.212	1378	3.3 - 4.1
J	11/09	1610	3	6.0	90.0	NH3 ph = 6.0	24.30	56.66	32.36	0.068	0.111	28.41		0.197	1139	3.9 - 4.8
K	11/09	1927	1	0.3	2.0	RURAL	5.43	5.43	0.00	0.067	0.164	0.00		0.231	471	5.1 - 5.3
L	11/09	2023	2	6.0	90.0	RURAL	4.96	5.68	0.72	0.049	0.232	0.89		0.288	804	4.5 - 4.7
M	11/10	1232	1	3.5	1.5	10 ppb H2O2	1.18	23.00	21.82	0.025	0.675	279.74		0.253	78	9.4 - 9.4

Gas phase concentrations of NH_3 and H_2O_2 were not measured. Since both of these gases are very soluble, most of the added gas was undoubtedly absorbed by the water on the walls and floor of the chamber. The aerosol mass before and after the cloud cycle are those calculated from the size distribution assuming that the aerosol is sulfuric acid [except for case J where the aerosol is assumed to be $(NH_4)_2SO_4$]. Since the RH in the DMA is approximately 34%, the sulfuric acid concentration and density of the aerosol are taken to be 50% and 1.4 g cm^{-3}, respectively. Control cloud-cycling experiments were carried out on October 31. These experiments detected no observable increase in aerosol mass when no reactants were added to the chamber or when SO_2, but no O_3 was added. There was a definite increase in the mass of the size distribution when both SO_2 and O_3 were added prior to a cloud cycle (results not included in Table 1).

If significant in-cloud conversion occurs, those particles which were activated in the cloud increase their acidic mass, causing a separation (local minimum) in the size distribution. Thus the critical radius separates those particles which had been activated in the cloud from those which existed as interstitial aerosol. From the location of the minimum, the activation radius, the maximum supersaturation in the cloud and concentration of cloud droplets can be inferred. These values are listed in the table for those data sets where detectable separation occurred.

Also listed in the table is the radius range of the PMS-CSASP channel where the peak concentration of droplets occurred at the time of maximum liquid water content (LWC). Two different radius ranges are given. One corresponds to the radii obtained using the manufacturer's calibration which was done using glass spheres of known radii. The other is an attempt to correct the calibration for the difference in refractive index between glass beads and water droplets using the data from Pinnick and Auvermann (1979). However, our PMS instrument is not identical to that used by these authors and the "corrected" radii, in our case, may not represent any improvement. Both values are given as an indication of the possible errors due to the uncertainties in refractive index in the CSASP calibration. In the radius range between 4 and 5 μm, very little difference exists between the factory calibration and the corrected one. However for all other channels, the correction was in a direction to lower the indicated radius. Cloud LWCs determined by IR extinction measurements are also given. The absolute concentrations of cloud droplets given by the PMS-CSASP were not reliable. The LWC calculated from the PMS-CSASP droplet spectra was normalized to the concentration of droplets inferred from the DMA and is given in Table 1 under the heading PMS/DMA. These values are always higher than those inferred from the IR extinction measurement given in the table. The IR-inferred LWC is believed to be the more accurate because small errors in the PMS-measured radius are magnified in calculating the volume of liquid water.

4.1 Liquid-Phase Conversion of Sulfur Dioxide to Sulfuric Acid by Ozone

This section discusses in detail the results of experiments on in-cloud conversion of SO_2 by O_3 for November 1, 2, and 9 (Figs. 8 through 15). On each of these days, there was large conversion of mass during the first cloud cycle resulting in a dramatic change in the size distribution as shown in Figs. 8, 11, and 15. While the total mass conversion shown in Figs. 8 and 15 (data sets B and H: 6.4 and 10.3 μg m^{-3}, respectively) was significantly higher than in Fig. 11 (data set E: 3.63 μg m^{-3}), the mass converted per cloud droplet was the largest for data set E where the cloud droplet radii were the largest. The average mass per droplet converted on November 1, 2, and 9 were 4.57, 29.9, and 6.88 femtograms, respectively. This can be explained by the fact that the cloud droplets formed during data set E were larger. According to Eq. (12) (and Fig. 1), the growth of the CCN should be controlled primarily by the cloud droplet radii.

To understand the change in the size distribution upon subsequent cloud cycling, we must look more closely at the size distribution.

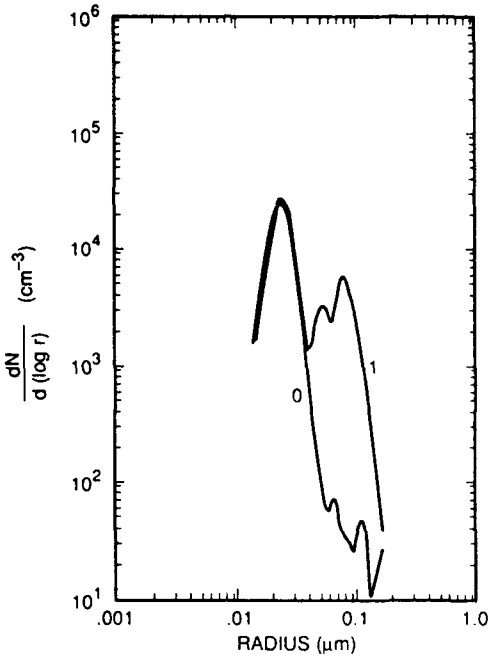

Fig. 8 — Changes in the aerosol size distribution during the first cloud cycle on November 1 (data set B). SO_2 and O_3 concentrations were 6.5 ppb and 107 ppb, respectively.

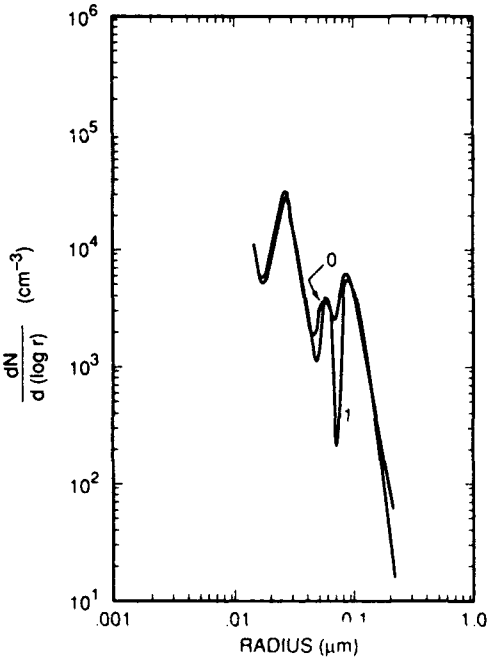

Fig. 9 — Changes in the size distribution during the second cloud cycle of November 1 (data set C). SO_2 and O_3 concentrations were 5.5 and 68 ppb, respectively.

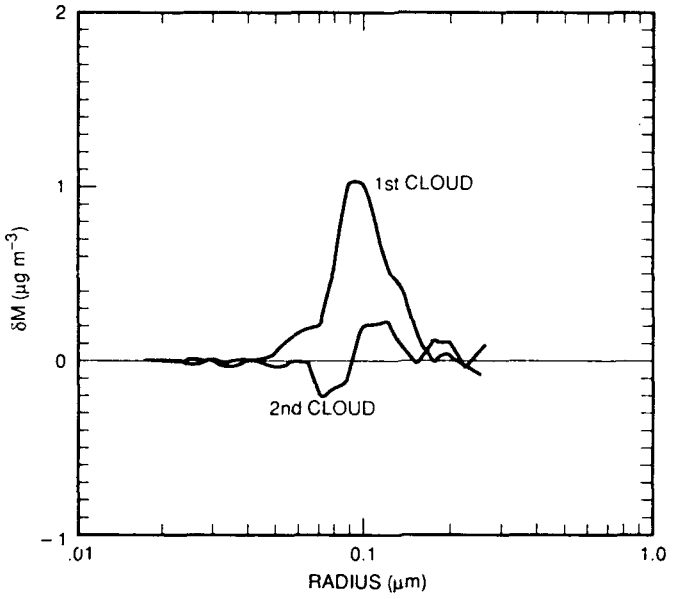

Fig. 10 — Difference in the mass (δM) before and after the first and second cloud cycles of November 1. δM is the mass change in each channel of the DMA plotted at the midpoint radius.

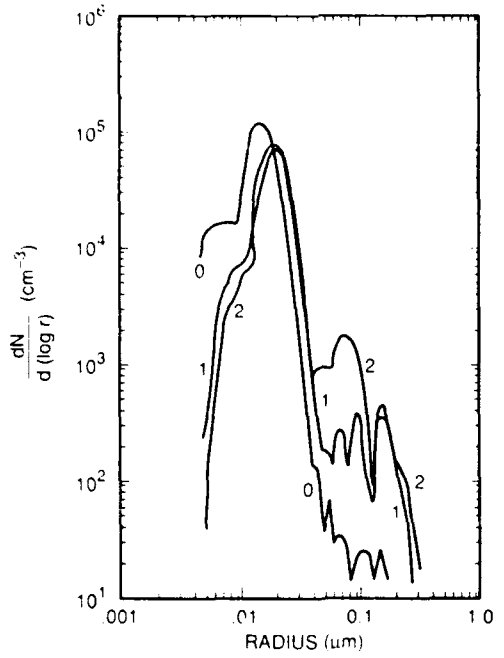

Fig. 11 — Size distributions prior to cloud formation and after the first and second cloud cycles on November 2

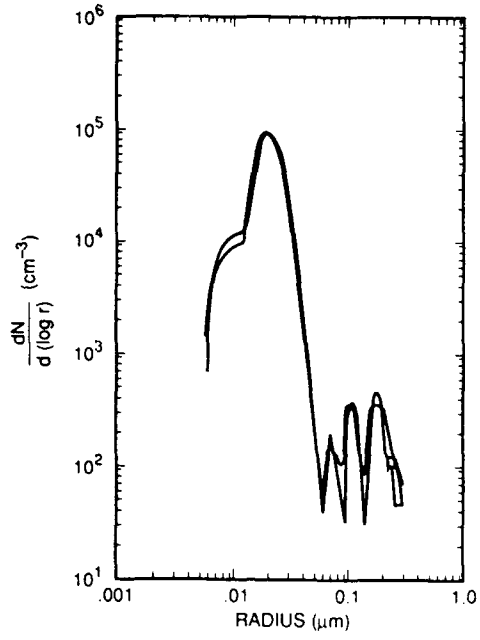

Fig. 12 — Three consecutive size distributions taken between the first and second clouds which show that three new peaks were formed during the first cloud on November 2

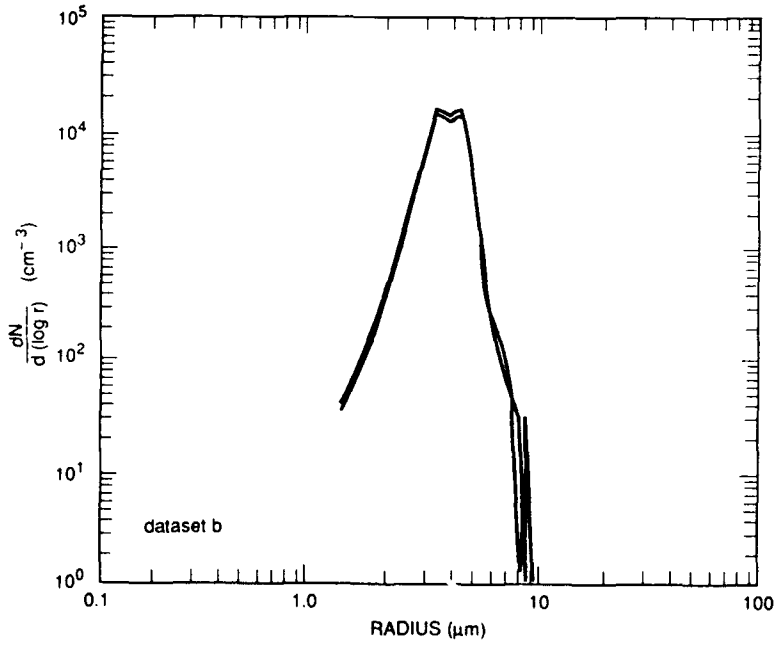

Fig. 13 — The cloud droplet size spectrum during the first cloud on November 1. Two peaks in the cloud droplet spectra correspond to the two peaks in the aerosol size distribution shown in Fig. 8, taken after the first cloud.

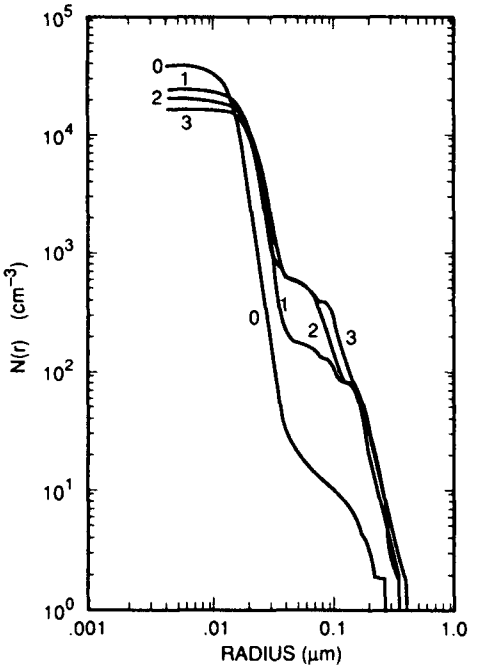

Fig. 14 — Same data as in Fig. 11, but displayed as cumulative size distributions, together with results of a third cloud cycle. Numbers on curves refer to size distributions taken after the numbered cloud cycle.

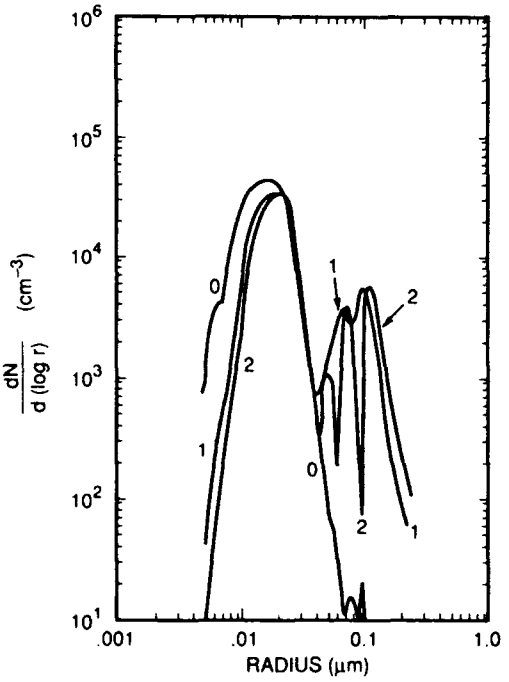

Fig. 15 — Size distributions measured before the first cloud cycle and after the first and second cloud cycles on November 9 (data sets H and I)

Figure 8 shows the change in the size distribution during the first cloud cycle on November 1 (data set B) when both O_3 (107 ppb) and SO_2 (7 ppb) were present in the chamber. There was a dramatic increase in the radii of particles whose original radii was greater than 0.04 μm. New peaks in the size distribution occurred at about 0.06 and 0.08 μm radii. From Fig. 1 (and Eq. (12)) we would expect particles of about 0.07 μm to be produced by the evaporated 5 μm radius droplets. For the second cloud, the expansion was somewhat slower, resulting in fewer cloud droplets of larger radius. While the PMS data showed that the droplets were only marginally larger (with the peak occurring in the same PMS channel as the first cycle), the change in the size distribution shown in Fig. 9 indicates that particles greater than 0.07 μm were activated and grew by a small amount, adding 0.4 $\mu g\ m^{-3}$ of mass to the size distribution and causing a break in the size distribution at 0.07 μm to deepen. While this behavior is difficult to detect in Fig. 9, it is clearly evident when the difference in mass before and after the cloud is plotted as a function of radius as shown in Fig. 10. Figure 10 shows the change in mass for each size channel of the DMA for both cloud cycles. For the second cloud cycle, the growth of particles in the 0.07 to 0.09 μm range removes them from that size range and moves them to the 0.10 to 0.13 μm size range, causing a modest increase in mass. The concentration of particles greater than about 0.2 is less than 10 cm^{-3} so that errors due to counting statistics in channels above 0.15 μm make the data above this size unreliable. A third cloud cycle was executed (data not shown) using an expansion rate similar to that used for the first cloud. The CSASP data indicated that the cloud droplet radii spectrum was the same as for the first cloud. No further conversion of mass was observed, presumably because the acidity of the cloud droplets due to the CCN upon which they formed was sufficient to block further conversion.

Figure 11 shows the differential size distribution prior to cloud formation and after the first and second cloud cycles for November 2. The oscillatory nature of the size distribution after the first cloud was real and not an artifact of the DMA data inversion scheme. The maxima and minima are in the raw data. This behavior occurred during many of the data sets, albeit usually not to the extent shown in Fig. 11 (see also Fig. 8). Figure 12 shows three consecutive size distributions taken between clouds 1 and 2 and demonstrates both the stability of the size distribution in the chamber and the high resolution of the DMA operating in the 44-channel scanning mode.

The multiple peaks appear to be associated with peaks in the cloud droplet spectrum measured with the CASAP. Figure 13 shows the cloud droplet size spectrum for the cloud that produced the two new peaks shown in Fig. 8 during the first cloud cycle. We do not know what caused the multiple peaks in the cloud droplet spectra; we know that they could not be identified with any features of the initial aerosol size distribution on which the droplets formed. The model, to be discussed later, did not display any multiple peaks in the cloud droplet spectra even though it used the measured expansion rate, included increase of solute by liquid phase conversion, and demonstrated "Ostwald ripening" in the aging cloud, processes which we thought might be responsible for the multiple peaks in the size distribution.

During the second cloud cycle also shown in Fig. 11, a faster expansion was employed. This produced a higher peak supersaturation which activated more particles with smaller radii. Those particles which were activated in the first cloud evidenced very little growth during the second cloud cycle, but the radii of newly activated particles increased to about 0.08 μm. This behavior can be explained by Figure 1. The first cloud had a droplet spectrum which peaked at about 8 μm and produced evaporated particles as large as 0.15 μm, whereas in the second cloud the peak in the droplet spectrum occurred at only 5.5 μm and produced particles of about 0.08 μm radius. The larger nuclei produced in the first cloud cycle provided sufficient acidity in the smaller droplets of the second cloud so that no further conversion could occur. Figure 14 shows the same data displayed as cumulative size distributions together with the results of the third cloud cycle. The cumulative size distribution enables display of multiple size distributions with less confusion. In the third size distribution, the peak at larger radii in Fig. 11 is preserved but the peak at 0.08 μm is split by growth of the larger particles associated with that

peak. This would indicate that the maximum supersaturation in the third cloud was somewhat less than that in the second cloud and that the cloud droplets in the third cloud were about 20% larger than in the second cloud. This does not necessarily contradict the data in the table which indicates that the PMS-CASAP channel containing the peak concentration of droplets is the same for both data sets. Closer examination of the droplet size distribution shows that the droplet spectrum was more sharply peaked at the larger sizes during the third cloud, whereas during the second cloud cycle, the spectrum was skewed to smaller sizes.

The decrease over time of the total aerosol concentration is the result of

- diffusional loss of interstitial particles to the cloud droplets during the cloud phase of the cycle, and
- "wall losses" during the period of several hours required to carry out several cloud cycles.

While the wall losses are small for the size range of interest here, they are larger than expected for a totally quiescent chamber because the mixing fan was left on at all times except during the period of cloud formation. Also, it should be pointed out that throughout the experiment slow particle growth was usually evident in the hour or so between cloud cycles. This was probably the result of continued gas-phase conversion similar to that used to produce the initial size distribution. All calculations of in-cloud conversion used the size distributions measured just before and after the cloud cycle. However, for purposes of displaying multiple cloud cycles we used just one of a number of size distributions taken between cloud cycles. For example, in Figs. 11 and 14, the size distribution used to illustrate the size distribution after the first cloud is really the size distribution measured just prior to the second cloud cycle. The slow growth during the hour and a half between clouds 1 and 2 causes the offset in the two size distributions in the size range around 0.02 to 0.03 μm. The change in the size distribution with time between clouds can be judged by Fig. 12 which shows three size distributions 10 min apart.

On November 3, cloud cycling data with SO_2 and O_3 in the chamber were taken but very little conversion was observed. At the time this was puzzling, since we had obtained dramatic results on the two previous days. However, subsequent analyses of the data showed that on November 3 the initial concentration was larger (over 1000 particles cm^{-3} larger than 0.05 μm and the expansion rates were such that cloud droplet concentrations were high and droplet radii mostly less than 3.5 μm. Figure 1 indicates that under these conditions conversion rates should be small. Therefore, the data from November 3 are not included in this report.

Figure 15 shows the results of the November 9 experiment (data sets H and I). In the first cloud cycle, about 10 $\mu g\ m^{-3}$ of material was formed with a peak concentration occurring at about 0.1 μm. This is at a somewhat larger size than we would have expected (see Fig. 1) for cloud droplets of the size ($\sim$4.5 μm) indicated by the PMS-CASAP. On the second cloud cycle, the initial expansion rate was slower, with the total expansion covering about the same time as the first. This produced a lower maximum supersaturation with fewer cloud droplets of larger radii ($\sim$5.5 μm). Only the larger nuclei in the previously formed peak grew, splitting the peak and forming a new peak at about 0.14 μm and adding about 4.5 $\mu g\ m^{-3}$ to the size distribution. Figure 16 shows the mass conversion for the two clouds as a function of size (DMA channel) for both cloud cycles. In the second cloud, particles larger than about 0.1 μm were activated and mass conversion resulted in growth to about 0.14 μm, causing a break in the size distribution. Again, under the assumption that all aerosol material is sulfuric acid, the size attained is larger than would be predicted for conversion in a 5.5 μm cloud droplet (see Fig. 1).

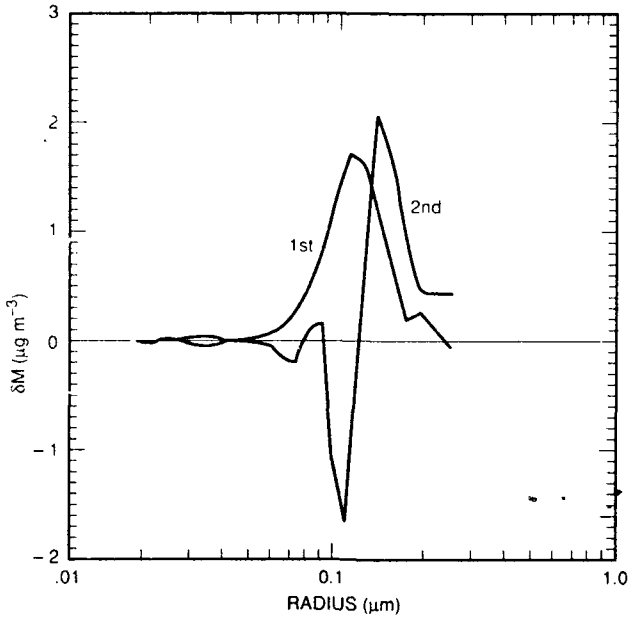

Fig. 16 — Change in mass as a function of radius during the two cloud cycles shown in Fig. 15. δM is the mass change in each channel of the DMA plotted at the midpoint radius.

4.2 Addition of NH_3 to the Chamber

On several occasions, gaseous NH_3 was added to the chamber before a third cycle to determine if the absorption of NH_3 by the cloud droplet would increase the pH of the droplets and result in additional conversion of SO_2 by O_3. After formation of the second cloud on November 9, sufficient NH_3 was added to the chamber to produce about 1 ppm if it all remained in the gaseous state. However, we believe most of the NH_3 dissolved into the liquid water on the walls and floor of the chamber. This water had been in contact with SO_2 and O_3 during the previous two cloud cycles and had undoubtedly become acidic. On previous occasions (end of day on November 2 and 3) when sufficient NH_3 had been added to the chamber to produce between 100 and 500 ppb if all remained in the gaseous state, subsequent cloud cycling showed no significant change in the size distribution. This result remains puzzling; we can only assume that the added NH_3 was depleted by dissolution in the liquid water before the cloud cycle was executed. As pointed out earlier, when SO_2 was added to the wet chamber, less than one third the calculated concentration appeared in the chamber as measured SO_2. As the day progressed, it was easier to maintain the SO_2 concentration. We interpret this as implying that the liquid water progressively came more into equilibrium with the gas phase reactants. However, prior to every new cloud cycle, additional distilled water was added to the chamber.

Figure 17 shows the size distributions taken before and after the third cloud cycle on November 9 when NH_3 was present with SO_2 and O_3. If we assume the aerosol (measured in the DMA) is dry $(NH_4)_2SO_4$ with a density of 1.77, 73 $\mu g\ m^{-3}$ were formed. We believe the very large conversion rate was due to the presence of the ammonia which neutralized the aerosol. There was some question regarding the measurement of SO_2 on this particular run but we estimate the SO_2 concentration to be about 6 ppb. This presents a dilemma because if the SO_2 concentration were 6 ppb, and if it were all converted to $(NH_4)_2SO_4$, the maximum yield would only be about 35 $\mu g\ m^{-3}$. The most likely explanation is that the $(NH_4)_2SO_4$ which existed as a solution particle at the high humidity in the chamber did not evaporate to dry size in the DMA. Tang (1980) indicates that $(NH_4)_2SO_4$ aerosol will not crystallize until the relative humidity has decreased to about 35%. For relative humidities between 30 and 40%, the

hydrated aerosol will have a radius (mass) about 1.3 (2.2) times greater than the dry particle (Tang 1980). If this were the case, the aerosol measured by the DMA would be 45% $(NH_4)_2SO_4$ by weight and the solution droplet would have a density of about 1.25. The total aerosol mass added to the size distribution would then be about 52 $\mu g\ m^{-3}$, of which 23 $\mu g\ m^{-3}$ would be $(NH_4)_2SO_4$, well within the bounds set by the available SO_2. As explained earlier, the humidity of the air sample enters the inlet tube through a diffusion dryer which lowers the relative humidity from ~100% to ~85%, at which point $(NH_4)_2SO_4$ particles are undoubtedly solution droplets. As the air enters the DMA proper, the humidity of the sample is further decreased because the humidity of the sheath air is about 30%. Whether or not the $(NH_4)_2SO_4$ particles crystallize at some point within the DMA is unknown.

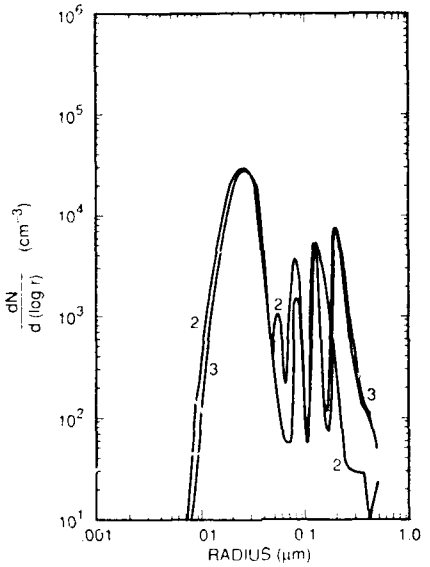

Fig. 17 — Change in the size distribution during the third cloud cycle on November 9 after NH_3 had been added to the chamber

4.3 Outside Air

At the end of the day on November 9 the chamber was flushed with outside air for an hour and 40 min before sealing the chamber. The chamber is located in a rural area of western New York State (near Springville, NY). It had been raining all day and the air was believed to be quite "clean". The CN concentration was 2000 cm^{-3}, and the measured gas concentrations were $[NO_x]$ = 11 ppb, $[O_3]$ = 3 ppb, and $[SO_2] = 0.5 \pm 0.5$ where the uncertainty for SO_2 is a result of the zero offset uncertainty. For the first cloud cycle (data set K) no reactants were added to the chamber and no change was observed in the size distribution. Before the second cloud cycle, SO_2 and O_3 were added to the chamber, increasing the concentrations to 6 ppb and 75 ppb, respectively. Figure 18 shows the size distribution before and after the cloud. The increase in mass was about 7 $\mu g\ m^{-3}$, more than doubling the original aerosol mass. Because the size distribution for outside air was much less steep than it was for artificially produced initial size distributions, the regions of particle removal are more graphically portrayed. Figure 19 shows the cloud droplet spectrum. The two peaks observed in the size distribution in Fig. 18 are ostensibly related to the two peaks in the droplet size distribution.

It is clear from Cases B-I and L, that there is no relationship between the mass conversion in the liquid phase and the liquid water content for cases when O_3 is the dominant oxidant.

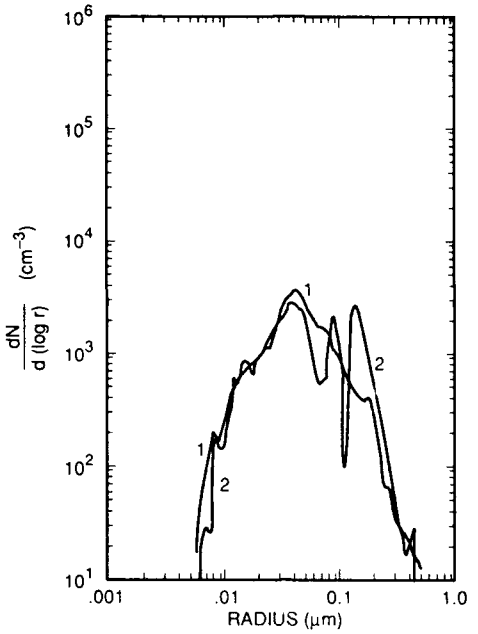

Fig. 18 — Chamber flushed with outside air. Size distribution 1 is distribution in outside air. Size distribution 2 is size distribution after a cloud cycle where SO_2 and O_3 concentrations of 6 ppb and 75 ppb had been added to the chamber.

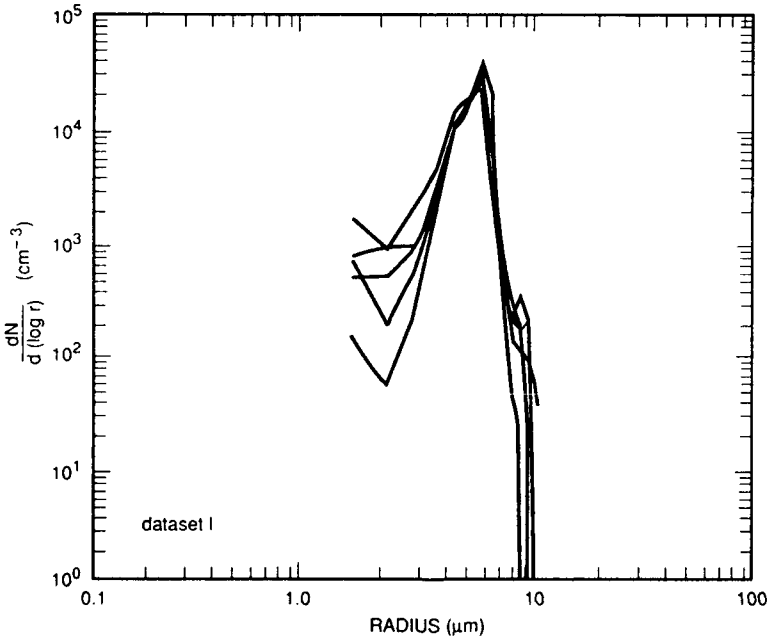

Fig. 19 — Cloud droplet size distribution during cloud cycle corresponding to Fig. 18. The double peaks in Fig. 18 are believed to be related to the peaks in the droplet spectrum at 3.5 and 5 μm.

4.4 Relationship Between Peaks in the Size Distribution and Peaks in the Cloud Droplet Spectrum

As shown in Section 2 for liquid phase conversion of SO_2 to sulfuric acid by O_3, the radial growth of the equivalent dry radius should be limited primarily by the size of the cloud droplet. This should be true for conditions, such as existed in our experiment, where there is sufficient SO_2 to lower the pH of the cloud droplet (to about 4) without expending the SO_2. Table 2 lists the radii where the peaks occurred in the aerosol size distribution and the ratio of the particle radius to the radius where the corresponding peak occurred in the droplet spectrum. Two sets of values are given: one where the factory calibration is used to determine droplet radii, the other where the (uncertain) correction for the index of refraction for water is used. In cases where multiple peaks could be positively identified, the values for the multiple peaks are also given. However, it should be pointed out that in every case, mass conversion at the largest radii far exceeded the mass conversion at the smaller radii. For this reason and because the largest peak is most easily detected and most persistent throughout the life of the cloud, the values for the largest peaks are believed to be more accurate. However, it is interesting to note that the average ratio for the second peaks is very nearly the same as the average ratio for the largest peaks. The values of the ratios shown in Table 2 can be compared to the value (0.0137) given by Eq. (13). While all the values are within a factor of two of each other, the values in the table are significantly higher than predicted by Eq. (13). Equation (13) can be written as

$$\frac{r}{R} = 0.58\,(k_2 K_1 K_2\, H_O H_S\, P_O P_S t)^{1/9} = 0.0137, \qquad (13')$$

Table 2 — Ratio of Radii Peaks in Aerosol and Droplet Distributions

DATA SET	PEAK	r_p (μm)	r_p/R_p F.C.	r_p/R_p P.C.	$\left(\frac{r_p}{R_p}\right)_{FC} + 0.0137$
B	1	0.085	0.017	0.018	1.24
	2	0.060	0.017	0.017	1.24
C	1	0.090	0.018	0.019	1.31
E	1	0.150	0.018	0.021	1.31
	2	0.098	0.015	0.017	1.09
F	1	0.090	0.018	0.019	1.31
G	1	0.110	0.019	0.022	1.39
H	1	0.110	0.030	0.031	2.19
	2	0.070	0.028	0.039	2.04
I	1	0.120	0.028	0.025	2.04
L	1	0.130	0.027	0.027	1.97
	2	0.240	0.024	0.024	1.75
	1	AVG.	0.022	0.023	1.60
	2	AVG.	0.021	0.024	1.53

r_p - Radius where peak occurs in aerosol size distribution
R_p - Radius where peak occurs in cloud droplet spectrum

where the notation is the same as that given in Section 2. The last column of Table 2 gives the factor by which the ratio (using the factory calibration value) differs from the predicted ratio of 0.0137. Because of the ninth root, any errors in the product ($k_2K_1K_2H_SH_OP_SP_Ot$) must be much larger than indicated in the works from which the constants (k_2,K_1,K_2,H_S, and H_O) were taken or larger than expected errors in the measurements of P_S, P_O, or time in cloud. For example, an error of a factor of 20 in the above product would translate to only a 40% error in the ratio. Of course, agreement with the predicted value could be obtained if either the cloud droplet radii indicated by the PMS optical counter were smaller, or the aerosol size indicated by the DMA were larger, by the factor given in the last column of Table 2. Possible explanations for the differences in the measured and predicted ratios are discussed later.

4.5 Liquid Phase Conversion of Sulfur Dioxide to Sulfuric Acid by Hydrogen Peroxide

On November 10, 1990, cloud cycling experiments using H_2O_2 instead of O_3 as the oxidant were carried out. Since the liquid-phase oxidation of SO_2 by H_2O_2 is nearly independent of pH, the growth of the acidic residue (equivalent dry radius) should not be limited by the pH of the cloud droplet as it was in the case of the SO_2-O_3 reaction. To inject H_2O_2 into the chamber, pure zero air was passed over a known solution of H_2O_2 until the air was in equilibrium with H_2O_2 and H_2O vapor pressure of the solution before entering the chamber. Unfortunately, there was no measurement of the gas-phase concentration of H_2O_2 in the chamber. Since H_2O_2 is very soluble, most of the H_2O_2 is believed to have dissolved in the liquid water on the walls and floor of the chamber. For the first cloud (data set M), H_2O_2 was injected into the chamber at a rate which would produce about 4 ppb per minute, for about 20 min. This would have produced 80 ppb of H_2O_2 in the chamber had none been lost to the walls and floor of the chamber. As stated earlier, we believe that only a small fraction of the 80 ppb actually remained in the chamber as gaseous H_2O_2. The 15 ppb of O_3 in the chamber as shown in Table 1, was the remnant of the ozone used to generate the background aerosol by the procedure described earlier. Figure 20 shows the size distribution before and after the cloud. For this case some of the aerosol particles grew beyond the range of the DMA (greater than 0.5 μm) so that the mass conversion of 23 μm m^{-3} shown in Table 1 represents the lower limit to the mass conversion. The concentration of cloud droplets was considerably lower than in most of the previously described data sets. The average conversion per cloud droplet was about 240 femtograms which is an order of magnitude higher than the highest conversion per drop for SO_2 oxidation by O_3, and even about 4 times greater than Case J where NH_3 was used to neutralize the acidity. A particle having a radius of about 0.04 and just activated in the cloud increased in radius to 0.4 μm in an 8 μm cloud droplet. Figure 21 shows the mass conversion as a function of radius. The H_2O_2 concentration required for the observed growth must be significantly greater than 1 ppb as shown in Fig. 5. If we assume that the H_2O_2 concentration was 10 ppb, then the ordinate in Fig. 5 would increase by a factor of $10^{1/3}$ and the observed increase in radius would agree with that predicted by Eq. (23).

Since the radii of the larger aerosol particles after the first cloud were too large to measure with the DMA, an attempt was made to remove them by forming a cloud while the mixing fan was running, thus impacting the cloud droplets on the walls and fan blade. This effort was not very effective. Nevertheless, a second cloud cycle was attempted and the results are given as data set N in Table 1. For the second cloud, only about half as much H_2O_2 was introduced into the chamber as in the prior cloud cycle. Because of the large number of larger particles existing prior to the cloud cycle and the possibility that a significant number of these particles grew too large to be detected by the DMA, the interpretation of data set N is uncertain.

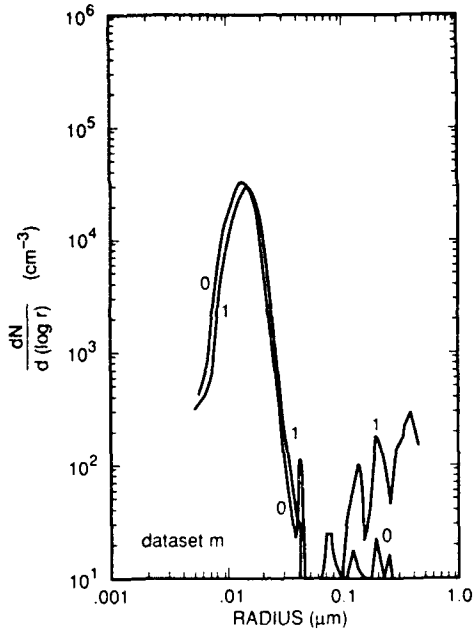

Fig. 20 — Size distribution before and after cloud cycle when H_2O_2 and SO_2 were reactants in the chamber (data set M)

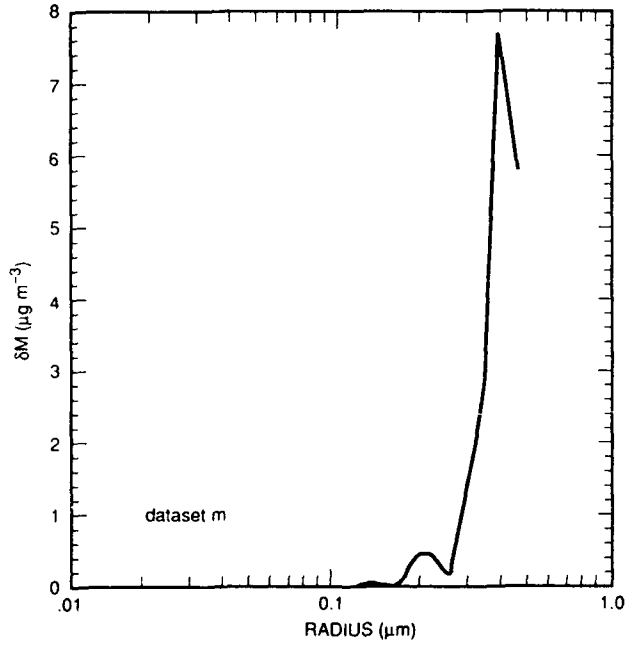

Fig. 21 — Mass conversion as a function of radius for the case shown in Fig. 20. δM is the mass change in each channel of the DMA plotted at the midpoint radius.

5. MODELING

Since cloud formation and concentrations of reactants in the chamber can be controlled and measured, the results described in Section 4 should be a good data set with which to compare modeled results. The following model used the measured expansion rate in the chamber and the measured initial aerosol size distribution (CCN spectrum) to predict the cloud droplet spectrum. The liquid-phase oxidation of SO_2 by O_3 (or H_2O_2) in the cloud droplets as given by the equations derived in Section 2 are used interactively to predict the change in the "dry" aerosol size distribution.

5.1 Description of Model

The change in the saturation ratio dS in the chamber produced by a given change in the pressure dP is

$$dS = \left\{1 - \frac{R'}{c_p}\left[25.2\left[\frac{273}{T}\right] - 5.31\right]\right\}\frac{dp}{p} - \left\{\left[25.2\left[\frac{273}{T}\right] - 5.31\right]\frac{L}{c_p T \rho_{air}} + \frac{1}{\rho_w^s}\right\} dM \tag{27}$$

where dM is the mass of liquid water (per cm^{-3}) formed during the change dP, L is the latent heat of water, c_p and R' are the heat capacity and gas constant for air in cal g^{-1} K^{-1}, ρ_{air} is the density of air, ρ_w^s is the water saturation vapor density, and T is the temperature. Substituting in the numerical values and taking $T = 293$ K, the change in the saturation ratio is

$$dS = -4.196\,\frac{dp}{p} - 1.841 \times 10^5\, dM. \tag{28}$$

The first term gives the change in the supersaturation if no liquid water were formed (as in an infinitely fast expansion), and the second term accounts for the changes in water vapor concentrations and latent heat during condensation or evaporation of droplets. The expansion is assumed to be adiabatic, i.e., no heat is transferred through the walls.

The formation of liquid water is governed by the droplet growth equation. In the model, the following form (Fletcher 1962) of the droplet growth equation is used:

$$\frac{dR_i}{dt} = \frac{D\rho_w^s}{\rho_w R_i}\left[S - \frac{A}{R_i} + \frac{B_o\, r_{idry}^3}{R_i^3}\right] \tag{29}$$

where R_i is the radius of a droplet in the i^{th} size class, S is the supersaturation, D the diffusion coefficient for water vapor, r_{idry} is the dry radius of the nucleus on which the droplets in the i^{th} class formed, and ρ_w is the density of water. The terms containing A and B_o account for the effects of surface tension and the vapor pressure lowering due to the solute in the CCN. In our experiments, the composition of the nucleus is well defined so that B_o will be the same for all particles. The total change in liquid water is obtained by summing the change over all droplet size classes

$$dM = 4\pi\rho_w \sum_i Z_i R_i^2 \left[\frac{dR_i}{dt}\right] dt \tag{30}$$

where Z_i is the number of cloud droplets in the i^{th} size class.

In the model, the size bins are defined by the midpoint radii of the 44 channels of the DMA; the bin boundaries are allowed to grow (or shrink) as would a particle of the same radius as the boundary. Thus a particle must always remain in the same size bin. The calculation is started at saturation ($S = 1$) where the particle (boundary) radius is given by

$$r_{is}^2 = \frac{B_o}{A} r_{idry}^3 \tag{31}$$

where r_{idry} is the radius at zero relative humidity (pure sulfuric acid). In the case of the DMA the measurements were made at about 34% RH where the particles are 50% sulfuric acid by weight and have a density of about 1.4. When the expansion begins, the radii marking the channel boundaries grow in accord with Eq. (29) and the change in liquid water (dM) is calculated from Eq. (30) and fed back into Eq. (28) at the next time step. Values of the pressure in the chamber were recorded every 10 s and these values are used to calculate the expansion rate required in Eq.(28). Figure 22 shows the growth of the channel boundaries and the evolution of the supersaturation with time for a typical expansion. Only the largest 26 of 44 channels are shown. The evolution of the supersaturation is also shown. The separation between the radii of unactivated and activated particles is clearly evident as the activated droplets grow. After the expansion is completed and the chamber is held at reduced pressure, the total liquid water remains constant. The end of the expansion is reflected by a small discontinuity in the supersaturation. One channel that was activated evaporated after the expansion was completed about 100 s into the cloud. As additional water vapor became available from the evaporating droplets, the supersaturation increased slightly. The liquid water from the evaporating droplets is transferred to the larger droplets (Ostwald ripening) and the supersaturation is determined by the supersaturation required to sustain the smallest size cloud droplets. Figure 23 shows the evolution of the computed cumulative droplet distribution at 30 s, 1, 2, 3 and 4 min after the beginning of the expansion for the simulation of data set H. The measured size distribution at 34% RH is shown, as is the size distribution adjusted to saturation (dotted line).

The agreement between the measured and calculated droplet distributions was usually quite good with respect to size. However, the concentrations measured with the PMS instrument were always larger than the computed value, much larger than the concentration required to obtain agreement with the total liquid water measured by Calspan's infrared extinction measurement, and larger than the concentrations inferred from the breaks in the aerosol size distribution as discussed in Section 3. We therefore accept the accuracy of the normalized PMS size distribution, but not the absolute value of concentration. This would imply that the manufacturer-determined sensing volume or air flow of the PMS was inaccurate. Since all of the expansions were in the 8 to 16 mb range, the maximum liquid water content for an adiabatic expansion (starting at saturation) must be in the range of 0.18 to 0.36 g m^{-3} (obtained directly from Eq. (28) by setting $dS = 0$). Since the chamber was slightly subsaturated at the start of the expansion, the liquid water contents must be below these maximum values. The values given by the Calspan IR liquid water measurement were always below the maximum value, but the values calculated from the PMS droplet spectra normalized to the concentration implied from the break in the DMA size distribution exceeded the maximum theoretical value on several occasions. The modeled values of liquid water were, of course, always correct for the given expansion and served as an integral check on the accuracy of the numerical solution (Eq. (28)).

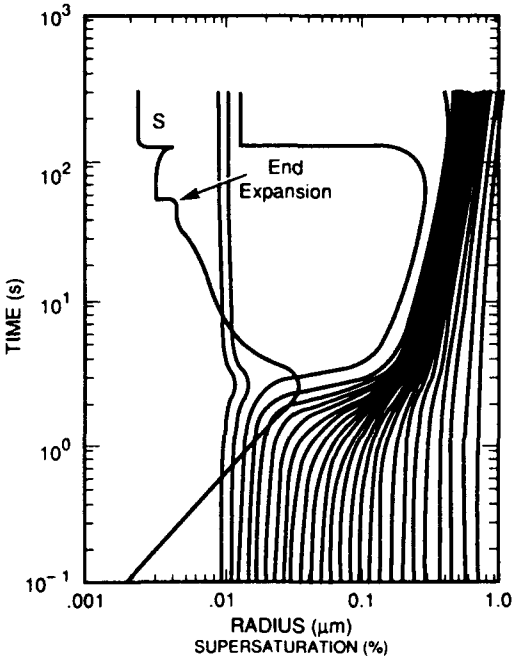

Fig. 22 — Growth of channel boundaries during cloud formation for a typical expansion. S is the supersaturation. This particular example was for data set B.

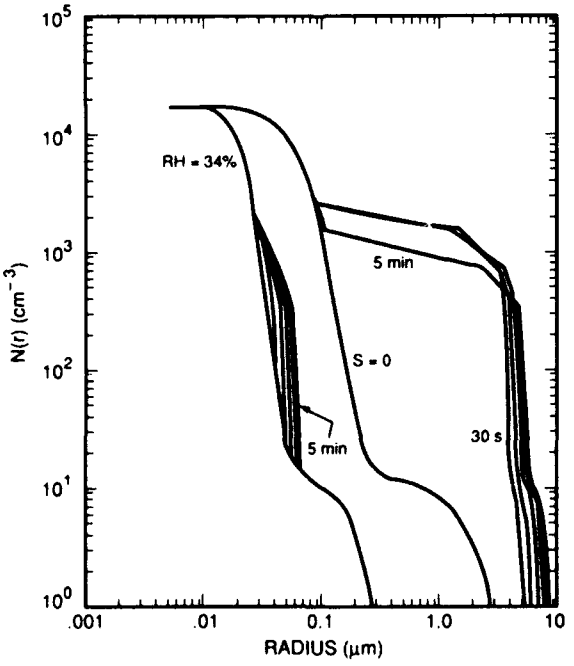

Fig. 23 — Evolution of cumulative size distribution as the larger aerosols are activated and grow to cloud droplet sizes. The initial size distribution is the measured dry size distribution. Smaller unactivated particles are plotted at both their "dry" size and size at saturation (S = 0).

Using the results of the previous section on aerosol growth laws, it is straightforward to add the liquid phase conversion of SO_2 to the model. Equation (5), for oxidation by ozone, or Eq. (20), for oxidation by H_2O_2, can be integrated at each time step to get the mass of sulfuric acid formed within the droplets. If vapor depletion is significant, then Eq. (26) is also incorporated into the calculation. The mass added due to liquid-phase conversion is used to recalculate the "dry radius" and the solute (last) term of Eq. (29) at each time step. Figure 23 also shows the growth of the "dry" radius due to liquid-phase conversion in the cloud droplets for Case B, to be discussed in the next section.

The small radii of the particles prior to activation (and the small radii of the unactivated particles) made it necessary to use a very small time step in the integration of the droplet growth equation. Numerical solutions simulating 4 to 5 min of in-cloud conversion required about an hour to execute on a 486-type personal computer running at 33 MHz. The program was written in compiled version of Quick Basic. To speed up the computations, aerosol particles which were several channels smaller than the smallest size for activation were ignored and they remained at their size at saturation. It was verified that this assumption had no effect on the solution; i.e., the amount of additional water taken up by the unactivated particles during the cloud cycle is negligible, as is the liquid-phase conversion in unactivated particles.

5.2 Model Results for Specific Runs

The results of the modeling are summarized in the second part of Table 1. For comparing how well the model simulated the measured parameters, the important parameters are the maximum supersaturation, and size and concentration of cloud droplets. As indicated earlier, the change in the size distribution can be used to indicate the maximum supersaturation in the cloud for those cases where measurable in-cloud conversion occurred. These experimentally determined supersaturations (Table 1(a)) can be compared to the model predicted supersaturations (Table 1(b)). The modeled and experimentally determined values of the maximum supersaturation track quite well but the modeled values are always somewhat higher. There is relatively good agreement in the measured and modeled cloud droplet size and this is reflected in Table 1 where the peaks in the modeled and measured spectrum correlate quite well. Figure 24 shows a typical comparison of measured and modeled cloud droplet size spectra at 2, 3, 4, and 5 min into the cloud (for data set B). Six measured droplet spectra were taken during the same time period but some are indistinguishable from each other (there appear to be only two) in Fig. 24. Ostwald ripening is clearly evident in the modeled result where growth of the larger particles continued even though the liquid water content is constant. The agreement is better using the radii from the factory calibration of the PMS-OPC rather than the radii from the attempt to correct for the refractive index of water. The size and number of droplets determines the total cloud liquid water content. As stated earlier, the concentration of droplets measured with the PMS-OPC is too large; only the radial distribution is assumed to be valid. The droplet radii intervals listed in Table 1(b) are the boundary channels containing the maximum number of cloud droplets at the time when the cloud has its maximum liquid water content, which is also given in Table 1(b).

We believe the agreement between the computed and measured cloud parameters is as good as can be expected considering the measurement errors involved in the PMS-OPC and considering the difficulty in selecting the critical radius by examining the change in the size distribution before and after cloud conversion. Any errors in selecting the size of the smallest particle activated affects the experimentally determined cloud droplet concentration and supersaturation given in Table 1(a). The total number of cloud droplets as determined from the break in the measured size distribution and the number predicted by the model show significant differences. This can be attributed to the steepness of the initial size distributions. As a result, the concentration of particles activated in the model is very sensitive to the expansion rate and to the amount of acid in the particles at the reference humidity. Even though our

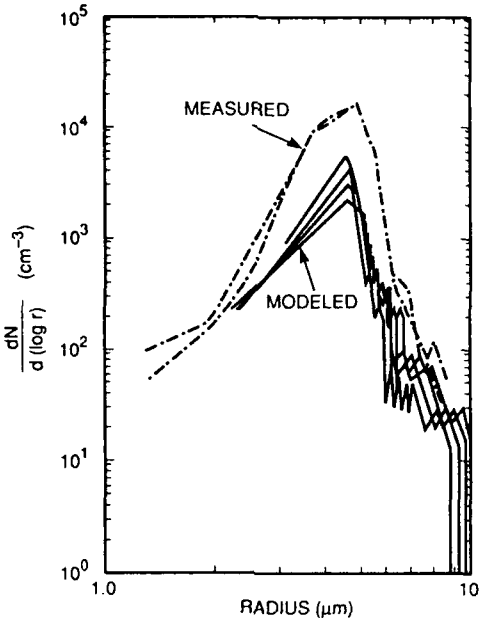

Fig. 24 — Comparison of measured and modeled cloud droplet spectra. Modeled results are plotted for 2, 3, 4, and 5 min. Measured spectra are six spectra taken during the same time period and several lie on each other making them impossible to resolve individually. Example is from simulation of data set B.

DMA was operating at very high resolution (44 channels), the steepness of the size distribution would often result in a factor of two change in the total cloud droplet population if one additional channel were activated.

The largest errors in the modeled cloud parameters stem from our inadequate knowledge of the exact relative humidity in the chamber prior to the expansion (due to finite accuracy of the dew point hygrometer) and to the rather coarse data on the expansion rate (pressure measurement every 10 s). Since the chamber is slightly subsaturated (by an unknown amount), a curve-fit to the pressure points was used to extrapolate back to the starting point of the expansion. In our calculations, it is assumed that saturation was achieved after 5 s of expansion, at which time model calculations began assuming a saturated chamber. As stated earlier, the duration of the expansion varied, but typically lasted about 1 to 1.5 min.

5.2.1 Modeled Results for Oxidation of Sulfur Dioxide by Ozone

The concentrations of reactants were measured only for the cases in which liquid-phase oxidation of SO_2 was by O_3. Therefore, only for data sets B, C, E, F, G, H, I, and L, can a comparison of modeled and experimental results be meaningful. As was discussed in the last section, the most dramatic changes occurred on the first cloud cycle on each of the three days when SO_2 oxidation by O_3 was studied. The results of all these runs are given in Table 1(b), but detailed results will be shown only for data sets B, E, and H, which were the first cloud cycles of each day, and data set L, which is data in air which contained natural aerosols as the starting size distribution.

The modeled change in the dry size distribution after 30 s, 1, 2, 3, 4, and 5 min are shown in Figs. 25 through 28 for data sets B, E, H, and L. The double-peaked characteristic caused by the mass conversion in cloud droplets is clearly present, but the total mass conversion is much smaller than the

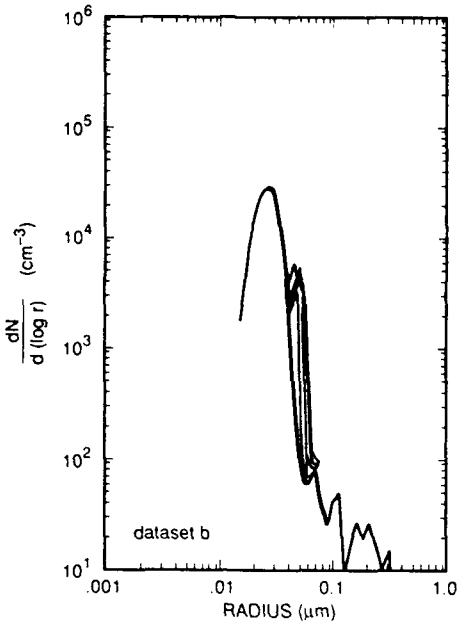

Fig. 25 — Modeled change in the dry (37% RH) size distribution for data set B at 0, 30 s, 1, 2, 3, 4, and 5 min

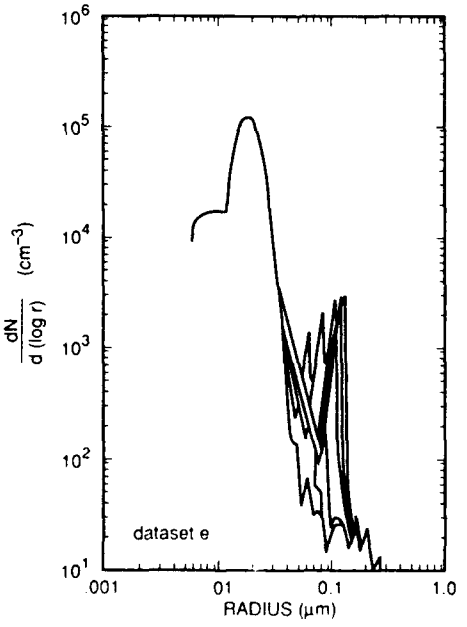

Fig. 26 — Modeled change in the dry size distribution for data set E at 0, 30 s, 1, 2, 3, 4, and 5 min

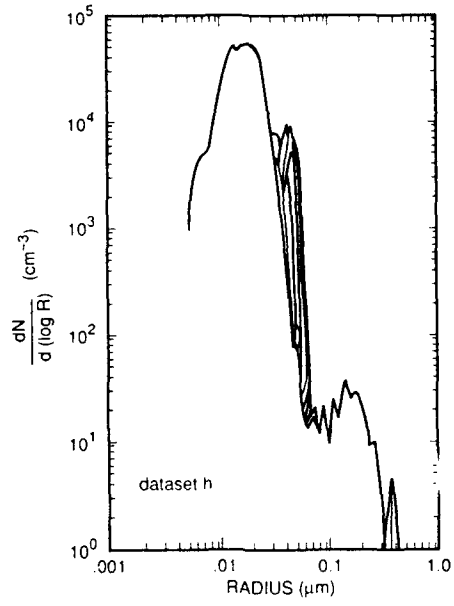

Fig. 27 — Modeled change in the dry size distribution for data set H at 0, 30 s, 1, 2, 3, 4, and 5 min

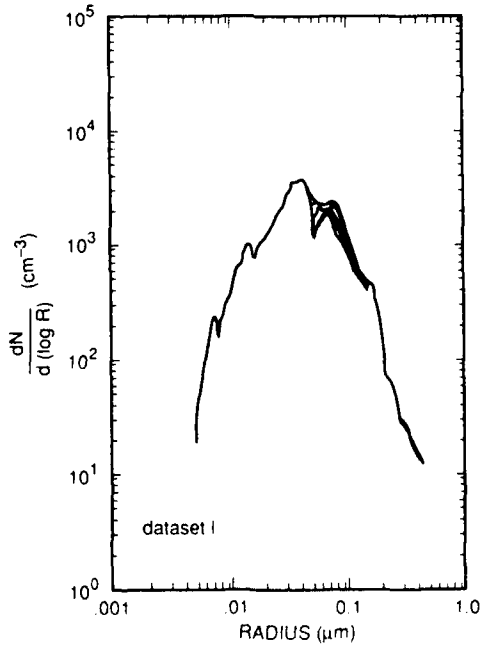

Fig. 28 — Modeled change in the dry size distribution for data set L at 0, 30 s, 1, 2, 3, 4, and 5 min

observed mass conversion shown in Figs. 8, 11, 15, and 18. For case E (Fig. 26), particle growth was largest because the cloud droplets were considerably larger than in cases B and H. For data set L (Fig. 28), the case when the aerosol was ambient aerosol from flushing the chamber with outside air, the initial aerosol was assumed to be nonacidic, but to have water absorption characteristics similar to sulfuric acid aerosol. In all other cases, the initial aerosol was assumed to be acidic.

Figure 29 shows the cumulative (dry) size distributions at 0, 30 s, 1, 2, 3, and 4 min for data set H. This is the same dry data as shown in Fig. 27 as a differential size distribution. Also shown in Fig. 29 is the cumulative measured size distribution after the cloud showing the large discrepancy between the measured and modeled conversion.

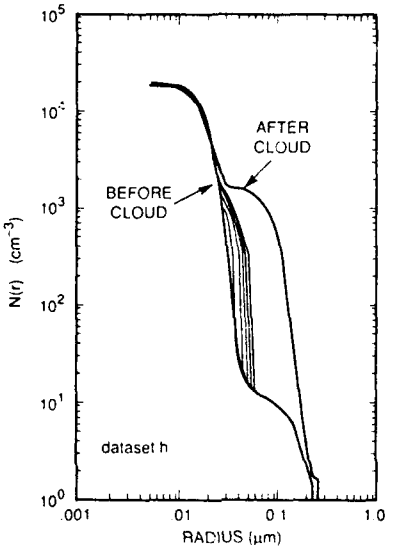

Fig. 29 — Cumulative distribution for simulation of data set H including the measured size distribution after the cloud

It is clear from Table 1 that the modeled change in the mass during the cloud cycles for these cases (SO_2 oxidation by O_3) was much lower than that actually measured; sometimes the modeled mass conversion was more than an order of magnitude smaller than observed. This is consistent with the results shown in Table 2 and the discussion in Section 4.4. When the constant in the second term of Eq. (5) was increased sufficiently to make the ratio of r/R given by Eq. (13′) to agree with the value of the ratio given in Table 2 (instead of the value 0.0137 given in Eq. (13)), then the agreement between the modeled mass conversion and observed mass conversion were quite good, as would be expected. The added mass using the adjusted constant is shown in the thirteenth column of Table 1(b) for data sets B, E, and H. However, this "forcing" of agreement between observation and modeling is unsatisfactory, since, as discussed in Section 4.4, the magnitude of the required change in the constant is larger than any anticipated errors in the experimentally determined parameters which make up this constant (in Eq. (5)). It does, however, show that the inferences of our simpler arguments given in Section 2.1, based only on the growth law and cloud droplet size, agree with the more rigorous model calculations.

The reason for the large discrepancy in mass conversion between the measured and modeled results is not known. It may be that the ozone generator (described in Section 3.3) which uses a high-voltage discharge, may have produced small concentrations of some unknown product such as H_2O_2 or some

excited molecule which, when dissolved in the cloud droplets, produced spurious oxidation of SO_2. For example, if in addition to producing 82 ppb of O_3 the generator also produced 2 ppb of H_2O_2 in the chamber, then the resulting conversion of SO_2 would have produced 10.4 $\mu g\ m^{-3}$ instead of 0.976 $\mu g\ m^{-3}$ of sulfuric acid aerosol for the case of data set H. The change in the modeled size distribution for data set H assuming 2 ppb of H_2O_2 is shown in Fig. 30 where it is compared to the measured change in the size distribution. This result is obtained by adding the conversion rate equations for O_3 and H_2O_2 oxidation of SO_2 (Eqs. (5) and (20)) in the model. Even though the concentration of O_3 is 82 ppb and H_2O_2 is only 2 ppb, the conversion is due primarily to the H_2O_2 and is limited by the availability of H_2O_2. This calculation (Fig. 30) is given to show that small amounts of unknown oxidants could produce the observed conversion. There is no way to know for certain what, if any, trace oxidants are formed by the O_3 generator without extensive tests on the output of the generator under the conditions of our experiments, where the output was introduced directly into a saturated chamber. These tests are beyond the scope of this investigation.

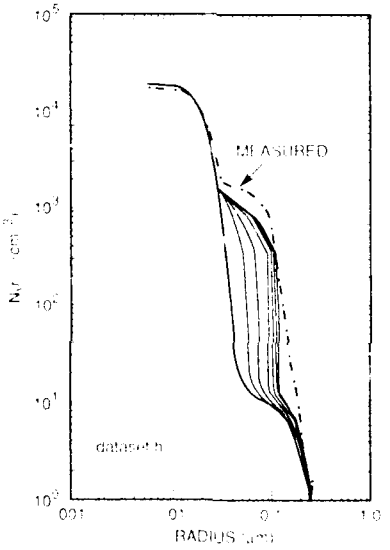

Fig. 30 — Modeled growth in the dry size distribution for data set H when 2 ppb of H_2O_2 is assumed to be present in addition to 82 ppb of O_3. Measured size distribution after the cloud is shown for comparison.

The above explanation loses some of its appeal when it is remembered that less conversion occurred on subsequent cloud cycles. This was explained in terms of the increased droplet acidity due to the increased size of the CCN on which the cloud droplet formed on subsequent cloud cycles. Before repeating a cloud cycle, the ozone generator was used to increase the O_3 concentration to the 70 to 100 ppb range. This "topping-off" of the ozone concentration required less ozone to be injected into the chamber than the initial injection, but any extraneous product produced by the generator would have also been injected before subsequent cloud cycles, and we would not have expected to see the pH limitation described in Section 3.

In a recent paper, Hansen et al. (1991) suggests that their data indicate that oxidation of SO_2 to sulfate in a dispersed system is different than in the bulk system, and that reaction rates in droplets may be quite different from those predicted by extrapolation of bulk solution results. Our results could be

interpreted as further experimental evidence to support this hypothesis. Until this hypothesis finds better theoretical foundation, we are reluctant to invoke it to explain our data.

A possible, but less probable, explanation of the discrepancy between modeled and measured conversion rates is that some ammonia may have been in the chamber. Ammonia used in the chamber on previous runs and removed by the charcoal filters could conceivably have been released during filtering to lower the concentrations of aerosols after the formation of the initial size distribution. No additional filtering was done over the number of hours during which the chamber was humidified and several cloud cycles were executed. Also, for the outside air sample (data set L) the air was not passed through the charcoal filters, and the observed conversion was still much higher than the modeled conversion.

A fourth possible explanation would be that the cloud droplet radii were larger than those indicated by the measurement with the PMS-OPC by the difference factor in Table 2 (factor of 10% to 100%). However, the rather good agreement between the measured and modeled values of cloud droplet radii and the constraint on the total liquid water content make this latter explanation improbable.

5.2.2 Modeled Results for the Case when Ammonia was Present

Data set J showed large conversion of SO_2 by O_3 when gaseous NH_3 was present. The NH_3 presumably dissolves in the droplets where it neutralizes the H_2SO_4 forming $(NH_4)_2SO_4$. The ammonium sulfate keeps the pH from dropping and facilitates oxidation of SO_2 by O_3 according to Eq. (2). If it is assumed that the presence of NH_3 only effects the pH ($[H^+]$) of Eq. (1), then the conversion rate of SO_2 to H_2SO_4 to $(NH_4)_2SO_4$ can be readily calculated by the model. The conversion rate is then given by

$$\frac{dM_a}{dt} = K R^3 P_O P_S \tag{32}$$

where K is 1.1×10^{12}, 1.1×10^{10}, or 1.1×10^{8} for pH of 7, 6, or 5, respectively. The model calculations were carried out for pH of 5, 6, and 7, and gave mass conversions of 0.86, 32, and 35 μg m^{-3}, respectively. If the water associated with the ammonium sulfate aerosol did not completely evaporate (as discussed in Section 4.2), the mass conversion as inferred from the DMA size distribution would be 1.92, 71 and 79 μg m^{-3}, respectively. For the case when pH = 6 and higher, the depletion of SO_2 was the dominant factor limiting conversion. For the case of pH = 7, the SO_2 was used up in about 10 s (invalidating the assumption of gas-liquid equilibrium). For the case of pH = 6, about 90% of the SO_2 was used up 4 min into the cloud, and for pH = 5, 2% of the SO_2 was used up 4 min into the cloud. There is a sharp cutoff in the conversion rate as the pH drops from 6 to 5. The modeled results for the case when the pH was assumed to be 6 is shown in Fig. 31, where the aerosol is assumed to be dry $(NH_4)_2SO_4$ with a density of 1.77. Also shown is the measured size distribution after the cloud.

5.2.3 Model Results for the Oxidation of Sulfur Dioxide by Hydrogen Peroxide

Liquid phase oxidation of SO_2 by H_2O_2 in a cloud was attempted on November 11 and the experimental results (data set M) are shown in Fig. 32. As discussed in Section 4.5, no measurements of H_2O_2 concentrations in the chamber were available, but H_2O_2 vapor could be injected into the chamber by flowing pure air over a solution of H_2O_2 at a rate which would result in a 4 ppb-per-minute increase. This was done for about 20 min prior to cloud formation for data set M. As stated earlier, we believe that only a small fraction of the H_2O_2 remains in the vapor state and most of the H_2O_2 was lost to the water on the walls and floor of the chamber prior to cloud formation. The model was run using Eq. (20) for the liquid phase conversion of SO_2 by H_2O_2, 3.5 ppb of SO_2, as measured just prior to cloud

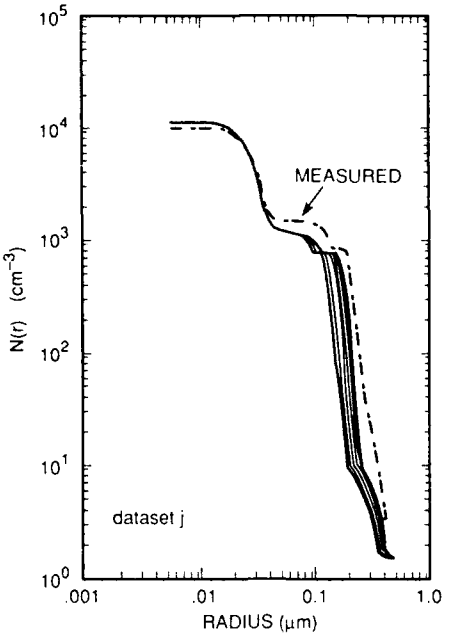

Fig. 31 — Modeled growth of the dry size distribution when the presence of NH_3 was assumed to hold the pH of the droplets at 6. The resulting aerosol is assumed to be dry $(NH_4)_2SO_4$. Measured size distribution after the cloud is shown for comparison.

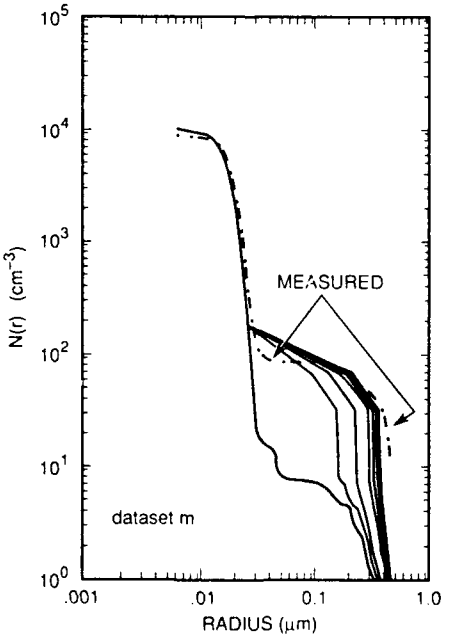

Fig. 32 — Modeled growth of dry size distribution using initial distribution from data set M. The SO_2 concentration is 3.5 and the concentration of H_2O_2 was assumed to be 10 ppb. Also shown is the measured size distribution after the cloud cycle.

formation, and for several assumed concentrations of H_2O_2. For 10 ppb and 2 ppb of H_2O_2, the mass conversions were 26.9 and 7.42 $\mu g\ m^{-3}$, respectively. The case for 10 ppb of H_2O_2 is shown in Fig. 31 and the result given in Table 1(b), case M. While the exact concentration of H_2O_2 is not known, it is clear that reasonable agreement between the measured and modeled size distributions can be achieved with reasonable values of H_2O_2. For the case of 10 ppb of H_2O_2, about 2.5 ppb of the H_2O_2 and SO_2 were consumed, whereas in the case of 2 ppb of H_2O_2, about 0.73 ppb of the H_2O_2 and SO_2 were consumed.

There appeared to be increased growth of the equivalent dry radius of the aerosol after SO_2 and H_2O_2 were added to the wet (but subsaturated) chamber. This phenomenon was not investigated in detail and usually the cloud was formed as soon after H_2O_2 injection as possible, so that the H_2O_2 would not be lost to the wet walls of the chamber. The growth of H_2SO_4 aerosol by oxidation of SO_2 by H_2O_2 in the high humidity (subsaturated) environment can be calculated from Eq. (20) where R is now interpreted as the equilibrium radius of the solution droplet at high humidity. The relationship between the radius of the solution droplet and the radius r_a of the pure acid particle after all water is removed can be written as

$$S = Exp\left\{\frac{A}{R} - \frac{B_o\, r_a^3}{R^3}\right\} \tag{33}$$

provided the saturation ratio is high enough ($0.85 < S < 1$) that the mass of the water is much greater than the mass of the pure acid. Expressing M_a in Eq. (20) in terms of the radius r_a, and using Eq. (33) to eliminate r_a gives a differential equation for R which has the solution

$$t = C_1\left[\frac{1}{R_o} - \frac{1}{R}\right] - C_2 \ln\left(R/R_o\right) \tag{34}$$

where R_o is the radius of the solution droplet at $t = 0$ and at a supersaturation S, and

$$C_1 = \frac{2A}{B_o}\left[\frac{3.9 \times 10^{10}\, P_S P_H}{4/3\ \pi\ \rho_a}\right]^{-1}$$
$$C_2 = 3(\ln S)\left[\frac{3.9 \times 10^{10}\, P_S P_H}{4/3\ \pi\ \rho_a}\right]^{-1}. \tag{35}$$

At any time t, the wet radius can be converted to the radius r_a of a pure acid particle by using Eq. (33).

Solutions to Eq. (34) for saturation ratios of 1, 0.995, 0.99, 0.98, and 0.95 are shown in Fig. 33 in terms of the pure acid radius, for initial radii of 0.1 and 0.2 μm and when $P_S = 10$ ppb and $P_H = 10$ ppb. Significant growth occurs over a 12 hour period only if the relative humidity is above about 98%, and for $S = 1$ the growth is very rapid.

The pH can be calculated by combining Eqs. (3) and (33)

$$\left[H^+\right] = \frac{(2.436)\ 4/3\ \pi\ \rho_a}{B_o}\left[\frac{A}{R} - \ln S\right]. \tag{36}$$

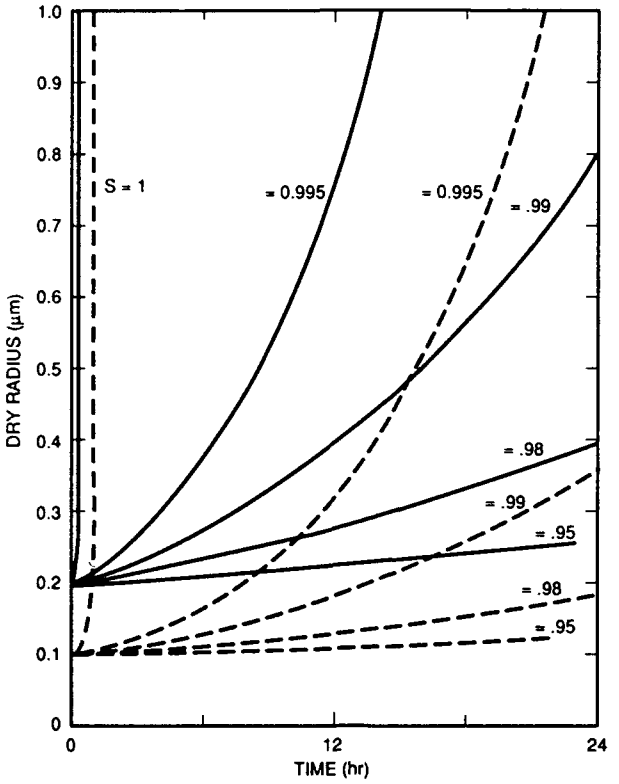

Fig. 33 — Growth of pure acid particle (water removed) at saturation ratios of 1.0, 0.995, 0.99, 0.98, and 0.95 in an environment where there is 10 ppb of both SO_2 and H_2O_2. Initial dry sizes are 0.1 and 0.2 μm.

The pHs calculated from Eq. (36) are below 2, which was stated earlier to be below the range of validity for Eq. (20). However, the conversion rates fall off rather slowly with decreasing pH (Martin 1984) and Eq. (20) can be considered correct within a factor of 2 for $1 < pH < 2$ and within a factor of 5 for $0 < pH < 1$.

This latter discussion has been included because questions regarding the possible importance of gas-to-particle conversion in wet aerosols (hazes) when the environmental humidity is high are often raised. Oxidation of SO_2 by H_2O_2 has sometimes been suggested as an important mechanism in the atmosphere because it can occur at low pH. Although high humidities can occur at the top of the planetary boundary layer, even when there are no visible clouds, and at ground level during the night due to radiative cooling, it seems unlikely that the very high humidities indicated here would prevail for long enough periods of time to make conversion by H_2O_2 important in the cloud-free atmosphere.

6. CONCLUSIONS

The cloud cycling experiments and modeling described in this report demonstrate that liquid-phase conversion of SO_2 in cloud droplets can have a dramatic effect on the aerosol size distribution. Observations of the aerosol size distribution before and after the aerosol has been processed through a (nonprecipitating) cloud is a very effective way of studying the liquid-phase conversion of trace gases in clouds. For the case when SO_2 and O_3 were introduced into the chamber, the observed conversion was clearly limited by the cloud droplet acidity produced by liquid-phase conversion of SO_2 to H_2SO_4 and by the acidity of the CCN on which the cloud droplet formed. The amount of conversion is a strong

function of the droplet radius. The dilution of acid in a large droplet raises the pH, resulting in rapid conversion of SO_2 and causing increased mass of the CCN after cloud evaporation.

Starting with well-established formulae for the oxidation of SO_2 by either O_3 or H_2O_2 in Henry's Law equilibrium with bulk water, growth laws for the increase in "dry" radius were derived. These chemical conversion formulations were used with a microphysical model of cloud formation to predict the change in the aerosol size distribution. The observed conversion for the case of SO_2 oxidation by O_3 was considerably larger than that calculated. The reason for the discrepancy between the observed and modelled conversion is not known but several possibilities were discussed in Section 5.2.1. The cause of the difference between the observed and predicted conversion rates should be explored further in future cloud chamber experiments.

The presence of (gaseous) NH_3, together with SO_2 and O_3, increased the liquid-phase conversion considerably. This undoubtedly is due to the fact that dissolved NH_3 reacted with H_2SO_4, increasing the pH of the droplet. The increase in pH promotes SO_2 absorption and oxidation of SO_2 within the droplet.

For the case of SO_2 oxidation by H_2O_2, no pH limitation to the conversion of SO_2 to H_2SO_4 was observed. The equivalent "dry" size of the aerosol increased dramatically and appeared to be limited only by availability of the gas-phase reactants.

An annoying aspect of the data was the multiple peaks in the size distribution often generated in a single cloud cycle. While these seemed to correlate with corresponding peaks in the cloud droplet spectrum, the accuracy and resolution of the cloud droplet spectrum was not adequate to verify that hypothesis conclusively. Furthermore, even if the multiple peaks in the cloud spectra are the cause, the source of the multiple peaks in the cloud spectra is not understood. Possible sources of the multiple peaks could be related to the dynamics of the expansion or preexisting "ripples" in the size distribution prior to cloud formation which were too small to be resolved by the DMA.

The equations given in this report can be used to make some general comments on the expected behavior of SO_2 concentrations in the remote marine boundary layer (MBL). In the following scenarios, we will assume that the flux of DMS (dimethyl sulfide) from the ocean is 140 μg S m^{-2} day^{-1} (Bates et al. 1987), that the DMS is converted uniformly in a 1 km MBL to give a SO_2 volume source rate of 3.2 $\times$ 10^{-18} g cm^{-3} s^{-1} and that DMS is the only source of SO_2. It is also assumed that the loss of SO_2 by in-cloud conversion is the primary loss mechanism. Ignoring loss by gas-phase conversion and surface deposition is obviously an oversimplification, but will give order-of-magnitude estimates for the effect of in-cloud conversion on SO_2 concentrations.

Scenario 1. Liquid-phase oxidation of SO_2 by O_3. Since the concentration of O_3 ($\sim$20 ppb) is much larger than that of SO_2, the O_3 concentration can be considered constant. Equations (5) and (26) can be written as

$$\frac{dM_a}{dt} = \frac{1.31 \times 10^{-3} R^9 P_O P_S}{M_a^2} \tag{37}$$

and

$$\frac{dP_s}{dt} = -228Z \frac{dM_a}{dt} + S_S \tag{38}$$

where S_S is the source of SO_2 from DMS (1.1×10^{-15} atm s^{-1}). If we assume that the clouds in the MBL consist of 100 droplets cm^{-3} of 10 μm radius (liquid water content of .42 g m^{-3}), and that a parcel of air spends one-twentieth of its time in a cloud, then the simultaneous solution to Eqs. (37) and (38) will give the SO_2 concentrations and the aerosol H_2SO_4 loading. Starting from zero concentrations, Fig. 34 shows the buildup of SO_2 and H_2SO_4 over the four days. During the first half-day, more of the SO_2 is converted to H_2SO_4 than remains as SO_2; however, at longer times, the conversion rate slows down and more sulfur remains as SO_2. This scenario produces only sulfuric acid aerosol and the concentration of SO_2 is greater after four days than is found in the remote MBL.

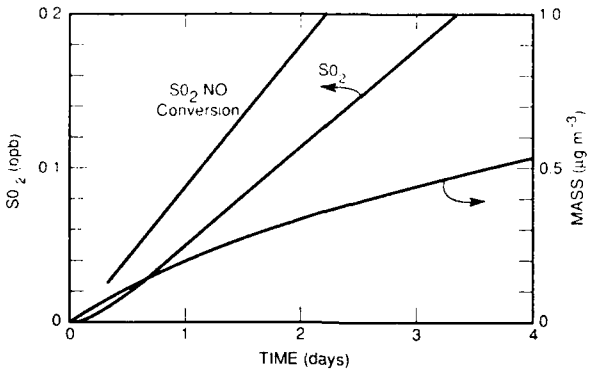

Fig. 34 — Concentrations of SO_2 and acidic mass assuming DMS is oxidized to SO_2 and SO_2 is converted to sulfuric acid by liquid-phase oxidation by O_3 within clouds. It is assumed that the air spends one-twentieth of its time in MBL clouds.

Scenario 2. SO_2 is oxidized by O_3 but NH_3 is present to partially neutralize the sulfuric acid. This is a distinct possibility since typical concentrations of NH_3 (0.2 ppb, Warneck 1986) found in the MBL are usually greater than typical SO_2 concentrations and NH_3 is more soluble than SO_2. As seen earlier (Section 5.2.2), the conversion rate depends strongly on the pH of the droplet. For fixed pH, the conversion rate is given by Eq. (32) where K depends strongly on the pH of the droplet. Equations (32) and (38) have a solution of the form

$$P_S = \frac{S_S}{C} - \left[\frac{S_S}{C} - P_S(o)\right] e^{-ct} \tag{39}$$

where $C = 195\, ZKR^3P_o$ is the reciprocal of the time for achieving equilibrium. For pH of 6, 5, and 4, the corresponding time constants are 1.2 hours, 5.4 days and 540 days; and the corresponding equilibrium concentrations of SO_2 are 0.005 ppb, 0.5 ppb, and 50 ppb. These calculations are based on the same cloud properties as Scenario 1 and a parcel of air spending one-twentieth of its time in a nonprecipitating cloud. It is clear that if NH_3 concentrations are large enough to keep the pH of the droplet as high as 6, then concentrations of SO_2 will be very low and most SO_2 will be converted to sulfate. In the other extreme, if the pH is as low as 4, the SO_2 concentrations will slowly build up to unrealistically high values.

Scenario 3. If oxidation of SO_2 in the remote MBL is by H_2O_2, then the depletion of H_2O_2 as well as SO_2 must be included. We were unable to identify any published measurements of H_2O_2 in the remote MBL; however, measurements at a number of locations, mostly over North America and Europe, are tabulated in review articles by Sakugawa et al. (1990) and by Gunz and Hoffmann (1990). Typical H_2O_2

concentrations in the MBL are probably of the same order of magnitude as are SO_2 concentrations, with both being highly variable. In the low NO_x environment of the remote MBL, H_2O_2 may well be greater than SO_2 concentrations.

Equations (20) and (38), which account for aerosol mass and SO_2 concentrations, can be augmented by the following equation to account for hydrogen peroxide

$$\frac{dP_h}{dt} = -228Z \frac{dM_a}{dt} + S_H \tag{40}$$

where S_H is the source strength of H_2O_2. Solutions to these three equations for the same cloud properties as in the prior scenarios and for MBL air spending one-twentieth of its time in a cloud are shown in Fig. 35. Solutions are shown for cases when the H_2O_2 source S_H are one-half, equal to, and double the SO_2 source strength. When the H_2O_2 source is larger than the SO_2 source strength, the SO_2 concentrations will be small.

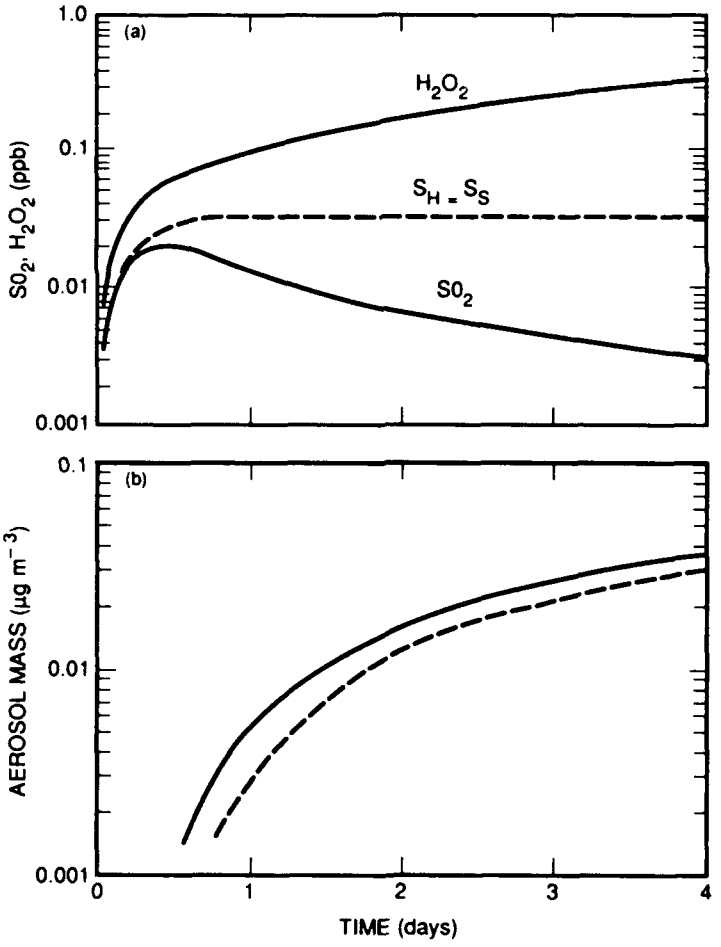

Fig. 35 — Concentrations of SO_2, H_2O_2, and aerosol mass when the source rate of H_2O_2 is twice as large as that for SO_2. If the source rate of H_2O_2 is half that of SO_2, then the curves for SO_2 and H_2O_2 are reversed. Dashed lines are for the case when the source rate of H_2O_2 is the same as that of SO_2.

In a more sophisticated chemical model of remote stratiform clouds, Chameides (1984) examines SO_2 conversion starting with fixed initial values of SO_2 and with H_2O_2 concentrations generated by the photochemical part of the model. When the initial SO_2 concentration was less than about 1 ppb, sufficient H_2O_2 was generated in the standard stratiform cloud model to convert all SO_2 to sulfate. Thus it would appear that H_2O_2 is more likely to predominate over SO_2 in the remote marine environment, resulting in very low SO_2 concentrations. This is in contrast to continental measurements made at two mountaintop sites in the Eastern U.S. (Meagher et al. 1990) where the SO_2 concentration was generally found to exceed the H_2O_2.

It is clear from the above three scenarios that if either NH_3 or H_2O_2 is present in concentrations which exceed that of SO_2, and if MBL clouds are present, then the concentration of SO_2 should be very low and loss by gas-phase and surface deposition will be low compared to liquid-phase conversion. If liquid-phase oxidation is primarily by O_3, then SO_2 concentrations would be higher than observed and loss by gas-phase oxidation and surface deposition would be required to account for the observed SO_2 concentrations. If liquid-phase conversion is important, as seems probable, MBL cloud cover should be an important parameter in determining ambient SO_2 concentrations.

ACKNOWLEDGMENTS

This research was supported by ONR, Code 12, through the "Transformation Dynamics of Aerosols" Accelerated Research Initiative.

REFERENCES

Bates, T.S., J.D. Cline, R.H. Gammon, and R.S. Kelly-Hanson. 1987. "Regional and Seasonal Variations in the Flux of Oceanic Dimethyl Sulfide to the Atmosphere," *J. Geophys. Res.* **92**, 2930-2938.

Chameides, W. L. 1984. "The Photochemistry of a Remote Marine Stratiform Cloud," *J. Geophys. Res.* **89**, 4739-4755.

Chylek, P. 1978. "Extinction and Liquid Water Content of Fogs and Clouds," *J. Atmos. Sci.* **34**, 296-300.

Finlayson-Pitts, B.J. and J.N. Pitts, Jr. 1986. *Atmospheric Chemistry: Fundamentals and Experimental Techniques* (Wiley-Interscience, New York).

Fletcher, N.H. 1962. *The Physics of Rainclouds* (Cambridge Press, Cambridge).

Gunz, D.W. and M.R. Hoffmann. 1990. "Atmospheric Chemistry of Peroxides: A Review," *Atmos. Environment* **24A**, 1602-1633.

Hansen, A. D. A., W. H. Benner, and T. Novakov. 1991. "Sulfur Dioxide in Laboratory Clouds," *Atmos. Environment* **25A**, 2521-2530.

Hegg, D.A., P.V. Hobbs, and L.F. Radke. 1980. "Observations of the Modification of Cloud Condensation Nuclei in Wave Clouds," *J. Rech. Atmos.* **14**, 217-222.

Hobbs, P.V. 1971. "Simultaneous Airborne Measurements of Cloud Condensation Nuclei and Sodium-containing Particles over the Ocean," *Quart. J. Royal Meteor. Soc.* **97**, 263-271.

Hoffmann, M.R. 1986. "On the Kinetics and Mechanism of Oxidation of Aquated Sulfur Dioxide by Ozone," *Atmos. Environment* **20**, 1145-1154.

Hoppel, W.A. 1978. "Determination of Aerosol Size Distribution from the Mobility Distribution of the Charged Fraction of Aerosols," *J. Aerosol Sci.* **9**, 41-54.

Hoppel, W.A. and G.M. Frick. 1990. "Submicron Aerosol Size Distributions Measured over the Tropical and South Pacific," *Atmos. Environment* **24A**, 645-659.

Hoppel, W.A. and G.M. Frick. 1986. "Ion-Aerosol Attachment Coefficients and the Steady-state Charge Distribution on Aerosols in a Bipolar Ion Environment," *Aerosol Science and Technology* **5**, 1-21.

Hoppel, W.A., J.W. Fitzgerald, and R.E. Larson. 1983. "Measurement of Atmospheric Aerosols: Experimental Methods and Results of Measurements off the East Coast of the United States," NRL Report 8703 (NTIS-ADA-130998).

Hoppel, W.A., G.M. Frick, and R.E. Larson. 1986. "Effect of Nonprecipitating Clouds on the Aerosol Size Distribution," *Geophys. Res. Letters*, **13**, 125-128.

Hoppel, W.A., J.W. Fitzgerald, G.M. Frick, R.E. Larson, and E.J. Mack. 1990. "Aerosol Size Distributions and Optical Properties Found in the Marine Boundary Layer over the Atlantic Ocean," *J. Geophys. Res.* **95**, 3659-3686.

Jacob, D.J. and M.R. Hoffman. 1983. "A Dynamic Model for the Production of H^+, NO_3^- and SO_4^{2-} in Urban Fog," *J. Geophys. Res.* **88**, 6611-6621.

Martin, L.R. 1984. "Kinetic Studies of Sulfite Oxidation in Aqueous Solution," in *SO_2, NO and NO_2 Oxidation Mechanisms: Atmospheric Considerations*, J.G. Calvert, ed. (Butterworth Publishers, Boston) pp. 63-100.

McMurry, P.H. and J.C. Wilson. 1982. "Growth Laws for the Formation of Secondary Ambient Aerosols: Implication for Chemical Conversion Mechanisms," *Atmos. Environment* **16**, 121-134.

Meagher, J. F., K. J. Olszyna, and F. P. Weatherford. 1990. "The Availability of H_2O_2 and O_3 for Aqueous Phase Oxidation. The Question of Linearity," *Atmos. Environment* **24A**, 1825-1829.

Overton, J.H., Jr. 1985. "Validation of the Hoffmann and Edwards' S(IV)-H_2O_2 Mechanism," *Atmos. Environment* **19**, 687-690.

Pinnick, R.G. and H.J. Auvermann. 1979. "Response Characteristics of Knollenberg Light-scattering Aerosol Counters," *J. Aerosol Sci.* **10**, 55-74.

Pruppacher, H.R. 1986. "The Role of Cloud Physics in Atmospheric Multiphase Systems: Ten Basic Statements," in *Chemistry of Multiphase Atmospheric Systems*, NATO ASI Series, W. Jaeschke, ed. (Springer-Verlag, Berlin).

Sakugawa, H., I.R. Kaplan, W. Tsai, and Y. Cohen. 1990. "Atmospheric Hydrogen Peroxide," *Environ. Sci. Technol.* **24**, 1452-1462.

Tang, I.N. 1980. "Deliquescence Properties and Particle Size Change of Hygroscopic Aerosols," in *Generation of Aerosols and Facilities for Exposure Experiments*, K. Willeke, ed. (Ann Arbor Science, Ann Arbor, MI) pp. 153-167.

Wang, S.C. and R.C. Flagan. 1990. "Scanning Electrical Mobility Spectrometer," *Aerosol Science* **13**, 230-240.

Warneck, P. 1986. *Chemistry of the Natural Atmosphere* (Academic Press, San Diego, CA).

Wu, C.H. and H. Niki. 1975. "Methods for Measuring the NO_2 Photodissociation Rate: Application to Smog Chamber Studies," *Environ. Sci. and Tech.* **9**, 46-52.